CRYSTAL GROWTH & DESIGN

Article

pubs.acs.org/crystal

First Tungstoantimonate-Based Transition-Metal–Lanthanide Heterometallic Hybrids Functionalized by Amino Acid Ligands

Jun-Wei Zhao,*[,†,‡] Jing Cao,[†] Yan-Zhou Li,[†] Jing Zhang,[†] and Li-Juan Chen*[,†]

[†]Henan Key Laboratory of Polyoxometalate Chemistry, Institute of Molecular and Crystal Engineering, College of Chemistry and Chemical Engineering, Henan University, Kaifeng, Henan 475004, People's Republic of China

[‡]State Key Laboratory of Structural Chemistry, Fujian Institute of Research on the Structure of Matter, Chinese Academy of Sciences, Fuzhou, Fujian 350002, People's Republic of China

Supporting Information

ABSTRACT: By the routine aqueous solution method, a series of transition-metal–lanthanide heterometallic tungstoantimonates $[Ln(H_2O)_8]_2[Fe_4(H_2O)_8(thr)_2][B\text{-}\beta\text{-}SbW_9O_{33}]_2\cdot 22H_2O$ [Ln = Pr^{III} (**1**), Nd^{III} (**2**), Sm^{III} (**3**), Eu^{III} (**4**), Gd^{III} (**5**), Dy^{III} (**6**), Lu^{III} (**7**), thr = threonine] were prepared and structurally characterized by multiple testing techniques. The common structural characteristic of **1**–**7** is that they are isomorphous and all consist of a $[Fe_4(H_2O)_8(thr)_2(B\text{-}\beta\text{-}SbW_9O_{33})_2]^{6-}$ subunit with two supporting $[Ln(H_2O)_8]^{3+}$ cations on both sides. It should be pointed out that two thr ligands in the $[Fe_4(H_2O)_8(thr)_2(B\text{-}\beta\text{-}SbW_9O_{33})_2]^{6-}$ subunit substitute for two water ligands in the classical $[Fe_4(H_2O)_{10}(B\text{-}\beta\text{-}SbW_9O_{33})_2]^{6-}$ polyoxoanion. As far as we know, **1**–**7** represents the first organic–inorganic tungstoantimonate hybrids consisting of transition metal and lanthanide cations and amino acid components. The fluorescence behavior of **4** has been measured and manifests the remarkable fluorescence feature resulting from the emission signature of Eu^{III} cations. Furthermore, the solid-state electrochemistry and electrocatalytic performances of **1** have been measured in 0.5 mol L^{-1} Na_2SO_4+H_2SO_4 aqueous solution, and the results show that **1** illustrates comparatively apparent catalytic activities toward the BrO_3^- and H_2O_2 reduction. The magnetic properties of **3** and **6** have been studied.

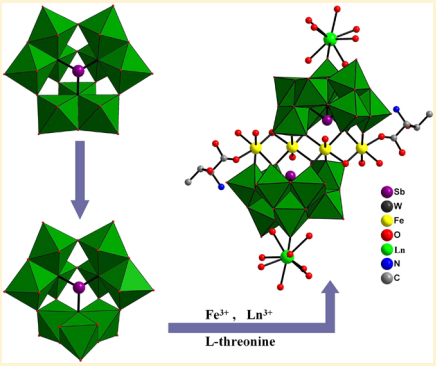

INTRODUCTION

Polyoxometalates (POMs) represent an special family of intriguing metal–oxygen cluster compounds formed by high oxidation state early transition metals (preferably Mo, W, V, and Nb) bearing tremendous diverse structures, seductive properties, and latent applications in catalysis, magnetism, electronics, photoluminescence, pharmaceutical, and materials science.[1−9] Highly negative charge, O-enriched lacunary POMs, can act as one kind of outstanding multidentate nucleophilic candidates to coordinate to transition-metal (TM) or lanthanoid (Ln) ions to construct neoteric TM or Ln encapsulated POM aggregates with varying metal centers, alluring topological architectures and novel properties, which can also make more magnetic or catalytic components implant to the POM cluster skeletons. Therefore, the exploration and discovery of TM- or Ln-functionalized POMs have attracted considerable interest over the past few decades. Hitherto, a vast amount of TM- or Ln-substituted POMs have been sequentially discovered.[10−19] In contrast, explorations on POM-based TM–Ln heterometallic derivatives (PTLHDs) still remain less developed, although their unmatched diversities and physicochemical properties entail them to become candidates for magnetic materials or optical sensing materials.[20−22] Less work dedicated to PTLHDs mainly lies in an inescapable competing reaction between electrophilic Ln and TM cations with nucleophilic POM precursors within a system.[23] Therefore, the search and preparation of POM-based TM–Ln heterometallic materials will remain a long-standing and persisting challenge. For all we know, since the first series of PTLHDs $[Ln(H_2O)_5\{Ni(H_2O)\}_2As_4W_{40}O_{140}]^{21-}$ (Ln = Y^{III}, Ce^{III}, Pr^{III}, Nd^{III}, Sm^{III}, Eu^{III}, and Gd^{III}) were discovered by Xue et al. in 2004,[24] some continuous findings were expanded.[25−37] In the past several years, we have made great efforts into this field and we have isolated several types of PTLHDs.[38−45] The majority of previously reported PTLHDs are inorganic or include some O- or N-containing organic ligands (such as tart, acetate, oxalate, ethylenediamine, 1,2-diaminopropane, 2,2′-bipyridine, 1,10-phenanthroline, pyrazine-2,3-dicarboxylate, etc.). However, there is no report on TM–Ln heterometallic tungstoantimonates (TAs) with amino acid ligands, which not only provides us with a big challenge and good opportunity but also exerts on us a strong impellent to develop this realm. With the goal of bringing in amino acid ligands to the PTLHD system, we recently have launched an exploration on the system of TAs, TM cations, Ln cations, and amino acid ligands. Albeit the family of Sb^{III}-inserting

Received: May 31, 2014
Revised: October 19, 2014
Published: October 27, 2014

polyoxotungstates has been known for several decades[46] and many TAs have been obtained,[47−57] no TA-based TM−Ln heterometallic species is reported. Therefore, the most crucial and used trivacant Keggin $[B\text{-}\alpha\text{-}SbW_9O_{33}]^{9-}$ precursor, which is formed by removing a W_3O_6 group from a plenary Keggin α-$SbW_{12}O_{40}$ unit, is selected as the candidate since (1) it is readily accessible and has relative high activity (the reactions between $[B\text{-}\alpha\text{-}SbW_9O_{33}]^{9-}$ and TM or Ln cations are summarized in Table S1 of the Supporting Information)[48−53,57−67] and (2) the lone electron pair stereochemical effect of the Sb^{III} atom in it to some extent precludes the closing of the Keggin units, which facilitates its combination with Fe^{3+} and Ln^{3+} cations and constructs novel PTLHDs with interesting properties. Amino acid ligands, which have flexible carboxyl and amino coordination sites, allow various coordination modes. Moreover, TM cations own the strong coordination ability toward both N- and O-donors, whereas Ln cations have priority to O-donors rather than N-donors in the light of the hard and soft acid and base rule, which can provide the large possibility for constructing novel structures. On the basis of the above ideas, Fe^{3+} and Ln^{3+} cations are simultaneously introduced to the $[B\text{-}\alpha\text{-}SbW_9O_{33}]^{9-}$ system in the participation of thr, which either can change the reactive behavior of the reactants or can deliver their luminescent and magnetic functional properties to the desired overcomes.[68−71] By trial and error, we have actually succeeded in making a group of novel PTLHD hybrids formulated as $[Ln(H_2O)_8]_2[Fe_4(H_2O)_8(thr)_2][B\text{-}\beta\text{-}SbW_9O_{33}]_2\cdot 22H_2O$ [Ln = Pr^{III} (**1**), Nd^{III} (**2**), Sm^{III} (**3**), Eu^{III} (**4**), Gd^{III} (**5**), Dy^{III} (**6**), Lu^{III} (**7**); thr = threonine] under bench conditions, which are characterized by elemental analyses, IR spectroscopy, X-ray photoelectron spectroscopy (XPS), and X-ray crystallography. Each of them contains a tetra-Fe^{III}-substituted sandwich-type $[Fe_4(H_2O)_8(thr)_2(B\text{-}\beta\text{-}SbW_9O_{33})_2]^{6-}$ hybrid subunit with two $[Ln(H_2O)_8]^{3+}$ pendant cations. Notably, comparing to the previously reported $[Fe_4(H_2O)_{10}(B\text{-}\beta\text{-}SbW_9O_{33})_2]^{6-}$ polyoxoanion,[48] two thr ligands supersede two water ligands, leading to the $[Fe_4(H_2O)_8(thr)_2(B\text{-}\beta\text{-}SbW_9O_{33})_2]^{6-}$ subunit in **1**−**7**. To our knowledge, they are the unseen TM−Ln heterometallic hybrid TAs with coordinate amino acid ligands. The photoluminescence of **4** has been measured and exhibits the characteristic emissions of Eu^{III} cations. Moreover, the electrocatalytic properties of **1** to the reduction of BrO_3^- and H_2O_2 have been evaluated in 0.5 mol L^{-1} sulfate aqueous media. To investigate whether the magnetic coupling can lead to the single molecule magnetic (SMM) behavior, the alternating current magnetic susceptibility measurements of **3** and **6** were performed.

EXPERIMENTAL SECTION

Materials and Methods. According to the literature method,[58] we synthesized $Na_9[B\text{-}\alpha\text{-}SbW_9O_{33}]\cdot 19.5H_2O$, which can also be proved by IR spectroscopy. Other chemicals were used as purchased without purification. C, H, and N elemental analyses were measured on a Perkin-Elmer 240C elemental analyzer. Inductively coupled plasma atomic emission spectrometry (ICP-AES) was carried out using a PerkinElmer Optima 2000 ICP-AES spectrometer. IR spectra were recorded using a powder sample palletized with KBr on a Nicolet 170 SXFT-IR spectrophotometer over the range of 4000−400 cm^{-1}. XPS analyses were obtained utilizing an Axis Ultra X-ray photoelectron spectrometer. Photoluminescence spectra and lifetime were recorded using an FLS 920P Edinburgh Analytical Instrument apparatus furnished by a 450 W xenon lamp and a μF900H high-energy microsecond flashlamp as the excitation sources. Cyclic voltametry measurements were performed on a Wuhan Corrtest CS-series electrochemical workstation at ambient temperature based on a three electrode system. The carbon paste electrode (CPE) acted as the working electrode; the counter electrode was the platinum gauze, and the referencing electrode was the Ag/AgCl electrode. The pH was adjusted using a PHB-4 pH meter. Magnetic susceptibility data were recorded on a Quantum Design MPMS XL−7 magnetometer in the temperature range of 1.8−300 K, and the magnetic data were corrected from diamagnetic contributions estimated from Pascal's constants.

*Synthesis of $[Pr(H_2O)_8]_2[Fe_4(H_2O)_8(thr)_2][B\text{-}\beta\text{-}SbW_9O_{33}]_2\cdot 22H_2O$ (**1**).* $Na_9[B\text{-}\alpha\text{-}SbW_9O_{33}]\cdot 19.5H_2O$ (0.200 g, 0.07 mmol) was dissolved in distilled water (15 mL) with stirring, and then $FeCl_3\cdot 6H_2O$ (0.032 g, 0.118 mmol), $PrCl_3$ (0.10 g, 0.40 mmol), and L-threonine (0.05 g, 0.42 mmol) were consecutively added. Using a dilute HCl solution (4 mol L^{-1}) adjusted the pH of the resulting solution to 1.20. The solution was stirred for 2 h, kept at 80 °C for 2 h, and then filtered (at this point, pH_s = 1.15) when it cooled to room temperature. The filtrate slowly evaporated at ambient temperature for several days, and green yellow cubic block crystals of **1** appeared (at this point, pH_e = 1.05). Yield: ca. 25% (based on $FeCl_3\cdot 6H_2O$). Elemental anal. Calcd for **1**: C, 1.55; H, 1.79; N, 0.45; Fe, 3.61; Pr, 4.56; Sb, 3.94; W, 53.54 (%). Found: C, 1.68; H, 1.92; N, 0.38; Fe, 3.49; Pr, 4.45; Sb, 4.02; W, 53.36 (%). IR (KBr, cm^{-1}): 3399 (s), 1627 (s), 1501 (w), 1395 (m), 1354 (w), 952 (s), 867 (w), 794 (s), 775 (w), 668 (m), 521 (w), 476 (w), and 420 (w).

*Synthesis of $[Nd(H_2O)_8]_2[Fe_4(H_2O)_8(thr)_2][B\text{-}\beta\text{-}SbW_9O_{33}]_2\cdot 22H_2O$ (**2**).* **2** was obtained employing a similar procedure to **1**, except that $NdCl_3$ (0.10 g, 0.40 mmol) replaced $PrCl_3$ (pH_s = 1.17, pH_e = 1.09). Yield: ca. 27% (based on $FeCl_3\cdot 6H_2O$). Elemental anal. calcd for **2**: C, 1.55; H, 1.79; N, 0.45; Fe, 3.61; Nd, 4.66; Sb, 3.94; W, 53.48 (%). Found: C, 1.64; H, 1.95; N, 0.36; Fe, 3.55; Nd, 4.49; Sb, 4.10; W, 53.34 (%). IR (KBr, cm^{-1}): 3408 (s), 1630 (s), 1499 (w), 1393 (w), 1343 (w), 950 (s), 868 (w), 794 (s), 765 (w), 667 (m), 526 (w), 476 (w), 427 (w)

*Synthesis of $[Sm(H_2O)_8]_2[Fe_4(H_2O)_8(thr)_2][B\text{-}\beta\text{-}SbW_9O_{33}]_2\cdot 22H_2O$ (**3**).* The procedure for the formation of **1** was employed, but $PrCl_3$ was replaced by $SmCl_3$ (0.10 g, 0.39 mmol) (pH_s = 1.14, pH_e = 1.08). Yield: ca. 32% (based on $FeCl_3\cdot 6H_2O$). Elemental anal. Calcd for **3**: C, 1.55; H, 1.79; N, 0.45; Fe, 3.60; Sm, 4.85; Sb, 3.93; W, 53.38 (%). Found: C, 1.43; H, 1.88; N, 0.34; Fe, 3.49; Sm, 4.71; Sb, 4.08; W, 53.26 (%). IR (KBr, cm^{-1}): 3406 (s), 1627 (s), 1499 (w), 1393 (w), 1343 (w), 950 (s), 875 (w), 804 (s), 768 (w), 662 (m), 525 (w), 467 (w), 420 (w).

*Synthesis of $[Eu(H_2O)_8]_2[Fe_4(H_2O)_8(thr)_2][B\text{-}\beta\text{-}SbW_9O_{33}]_2\cdot 22H_2O$ (**4**).* The synthetic procedure of **1** was utilized, but instead of $PrCl_3$, we used $EuCl_3$ (0.10 g, 0.39 mmol). Yield: ca. 32% (based on $FeCl_3\cdot 6H_2O$) (pH_s = 1.14, pH_e = 1.12). Elemental anal. Calcd for **4**: C, 1.55; H, 1.79; N, 0.45; Fe, 3.60; Eu, 4.90; Sb, 3.93; W, 53.35 (%). Found: C, 1.41; H, 1.89; N, 0.35; Fe, 3.52; Eu, 4.76; Sb, 4.06; W, 53.24 (%). IR (KBr, cm^{-1}): 3399 (s), 1630 (s), 1499 (w), 1393 (w), 1352 (w), 950 (s), 869 (w), 804 (s), 773 (w), 664 (m), 525 (w), 467 (w), 420 (w).

*Synthesis of $[Gd(H_2O)_8]_2[Fe_4(H_2O)_8(thr)_2][B\text{-}\beta\text{-}SbW_9O_{33}]_2\cdot 22H_2O$ (**5**).* **5** was prepared according to the method of **1**, but $GdCl_3$ (0.10 g, 0.370 mmol) was used instead of $PrCl_3$. Yield: ca. 32% (based on $FeCl_3\cdot 6H_2O$) (pH_s = 1.12, pH_e = 1.09). Elemental anal. calcd for **5**: C, 1.55; H, 1.78; N, 0.45; Fe, 3.60; Gd, 5.06; Sb, 3.92; W, 53.26 (%). Found: C, 1.39; H, 1.89; N, 0.33; Fe, 3.53; Gd, 4.90; Sb, 4.05; W, 53.16 (%). IR (KBr, cm^{-1}): 3399 (s), 1630 (s), 1495 (w), 1402 (w), 1352 (w), 945(s), 874(w), 794 (s), 770 (w), 663 (m), 519 (w), 476 (w), 422 (w).

*Synthesis of $[Dy(H_2O)_8]_2[Fe_4(H_2O)_8(thr)_2][B\text{-}\beta\text{-}SbW_9O_{33}]_2\cdot 22H_2O$ (**6**).* **6** was prepared similar to **1**, but $DyCl_3$ (0.10 g, 0.37 mmol) was used instead of $PrCl_3$ (0.10 g, 0.39 mmol) (pH_s = 1.09, pH_e = 1.06). Yield: ca. 32% (based on $FeCl_3\cdot 6H_2O$). Elemental anal. Calcd for **6**: C, 1.54; H, 1.78; N, 0.45; Fe, 3.59; Dy, 5.22; Sb, 3.91; W, 53.17 (%). Found: C, 1.42; H, 1.92; N, 0.36; Fe, 3.47; Dy, 5.05; Sb, 4.06; W, 53.09 (%). IR (KBr, cm^{-1}): 3397 (s), 1630 (s), 1499 (w), 1393 (w), 1352 (w), 950 (s), 870 (w), 774 (w), 804 (s), 660 (m), 525 (w), 467 (w), 422 (w).

Table 1. Crystallographic Data for 1−7

	1	2	3	4
formula	$C_8H_{110}Fe_4N_2O_{118}Pr_2Sb_2W_{18}$	$C_8H_{110}Fe_4N_2O_{118}Nd_2Sb_2W_{18}$	$C_8H_{110}Fe_4N_2O_{118}Sm_2Sb_2W_{18}$	$C_8H_{110}Fe_4N_2O_{118}Eu_2Sb_2W_{18}$
M_r (g mol^{-1})	6180.84	6187.66	6199.88	6203.10
space group	$P\bar{1}$	$P\bar{1}$	$P\bar{1}$	$P\bar{1}$
crystal system	triclinic	triclinic	triclinic	triclinic
a (Å)	12.6294(5)	12.6125(6)	12.6058(5)	12.6012(6)
b (Å)	13.6304(5)	13.5912(7)	13.5742(5)	13.5607(6)
c (Å)	16.3489(7)	16.2958(8)	16.2643(7)	16.2390(7)
α (deg)	107.2450(10)	107.0660(10)	106.9910(10)	106.9480(10)
β (deg)	99.9600(10)	100.0030(10)	99.9670(10)	99.9240(10)
γ (deg)	96.7130(10)	96.7300(10)	96.7560(10)	96.9080(10)
V (Å^3)	2604.68(18)	2587.5(2)	2579.25(18)	2571.5(2)
Z	1	1	1	1
D_c (g/cm^3)	3.940	3.971	3.992	4.006
μ (mm^{-1})	21.877	22.084	22.287	22.432
R_{int}	0.0349	0.0367	0.0395	0.0293
limiting indices	$-14 \le h \le 14$	$-14 \le h \le 14$	$-14 \le h \le 14$	$-14 \le h \le 14$
	$-15 \le k \le 16$	$-14 \le k \le 16$	$-16 \le k \le 14$	$-15 \le k \le 16$
	$-19 \le l \le 19$	$-18 \le l \le 19$	$-19 \le l \le 17$	$-19 \le l \le 11$
reflns collected	13394	13006	13321	13203
indep reflns	9038	8956	8995	8916
parameters	653	644	629	639
GOF on F^2	1.067	1.038	1.025	1.063
$R_1{}^a$, $wR_2{}^b$ [$I > 2\sigma(I)$]	0.0463, 0.1081	0.0795, 0.2215	0.0539, 0.1388	0.0393, 0.0927
$R_1{}^a$, $wR_2{}^b$ (all data)	0.0529, 0.1113	0.0845, 0.2269	0.0633, 0.1448	0.0435, 0.0948

	5	6	7
formula	$C_8H_{110}Fe_4N_2O_{118}Gd_2Sb_2W_{18}$	$C_8H_{110}Fe_4N_2O_{118}Dy_2Sb_2W_{18}$	$C_8H_{110}Fe_4N_2O_{118}Lu_2Sb_2W_{18}$
M_r (g mol^{-1})	6213.68	6224.18	6213.09
space group	$P\bar{1}$	$P\bar{1}$	$P\bar{1}$
crystal system	triclinic	triclinic	triclinic
a (Å)	12.6124(6)	12.5725(8)	12.5684(7)
b (Å)	13.5806(6)	13.5254(9)	13.4822(7)
c (Å)	16.2545(8)	16.1682(10)	16.0879(8)
α (deg)	106.8820(10)	106.6690(10)	106.5000(10)
β (deg)	99.9550(10)	99.9640(10)	99.8200(10)
γ (deg)	96.9010(10)	97.0380(10)	97.2780(10)
V (Å^3)	2580.8(2)	2550.6(3)	2530.9(2)
Z	1	1	1
D_c (g/cm^3)	3.998	4.052	4.076
μ (mm^{-1})	22.421	22.851	23.500
R_{in}	0.0454	0.0354	0.0310
limiting indices	$-14 \le h \le 14$	$-14 \le h \le 14$	$-14 \le h \le 14$
	$-16 \le k \le 13$	$-16 \le k \le 15$	$-16 \le k \le 12$
	$-18 \le l \le 19$	$-16 \le l \le 19$	$-19 \le l \le 17$
reflns collected	13221	13140	12715
indep reflns	8992	8881	8708
parameters	634	629	614
GOF on F^2	1.032	1.054	1.033
$R_1{}^a$, $wR_2{}^b$ [$I > 2\sigma(I)$]	0.0530, 0.1384	0.0499, 0.1273	0.0658, 0.1878
$R_1{}^a$, $wR_2{}^b$ (all data)	0.0572, 0.1415	0.0541, 0.1301	0.0697, 0.1918

Synthesis of $[Lu(H_2O)_8]_2[Fe_4(H_2O)_8(thr)_2][B\text{-}\beta\text{-}SbW_9O_{33}]_2{\cdot}22\ H_2O$ (7). The preparation of **7** was similar to that of **1**, except that $LuCl_3$ (0.10g, 0.27 mmol) was in place of $PrCl_3$ (pH_s = 1.17, pH_e = 1.09). Yield: ca. 32% (based on $FeCl_3{\cdot}6H_2O$). Elemental anal. Calcd for **7**: C, 1.54; H, 1.77; N, 0.45; Fe, 3.57; Lu, 5.60; Sb, 3.90; W, 52.96 (%). Found: C, 1.40; H, 1.94; N, 0.34; Fe, 3.43; Lu, 5.45; Sb, 4.03; W, 53.07 (%). IR (KBr, cm^{-1}): 3397 (s), 1630 (s), 1499 (w), 1393 (w), 1352 (w), 950 (s), 804 (s), 652 (m), 525 (w), 467 (w), 422 (w).

X-ray Crystallography. High-quality crystals of **1**−**7** were picked up from their mother liquors and mounted on the fiber glass. Intensity data were collected on a Bruker Apex II diffractometer equipped with CCD area detector using monochromated Mo Kα radiation (λ = 0.71073 Å) at 296 K. Data reduction were executed by the SAINT software suite.[72] On the basis of multiple and symmetry-equivalent reflections in the data set, the absorption correction was employed utilizing SADABS.[73] Their structures were determined by direct methods by means of SHELXTL-97.[74,75] Those H atoms bonding with H_2O were not located from the Fourier syntheses. H atoms associated with C and N atoms were placed in calculated positions using a riding model and were refined isotropically using the default SHELXTL parameters. The crystal data and structure refinement parameters for **1**−**7** are summarized in Table 1.

dx.doi.org/10.1021/cg5007988 | Cryst. Growth Des. 2014, 14, 6217−6229

RESULTS AND DISCUSSION

Synthesis. In the past several years, we have succeeded in utilizing the synthetic approach of lacunary POM precursors reacting with TM/Ln ions and appropriate multidentate organic ligands under hydrothermal environments and resulted in several types of inorganic−organic hybrid PTLHDs.[7] As a part of our continuous work, we anticipate obtaining novel PTLHDs with amino acid ligands because amino acids as one kind of O- and N-containing organic ligands with strong coordination ability can replace other O- or N-containing organic ligands to participate in constructing polynuclear TM clusters and high-dimensional structures.[76−79] Thus, amino acid ligands were used during the preparation of novel PTLHDs. Furthermore, as the basic ingredients of proteins, amino acids are water-soluble, commercially available and nontoxic,[80] and also have an intimate relationship to the organism's life activities for studying in medical applications.[81,82] Up to now, some Ln−amino acid complexes and TM−amino acid complexes have been synthesized.[83−86] All these suggest that amino acids are useful ligands; however, reports on POMs with amino acids are underdeveloped,[87−96] although researchers have devoted great efforts to the reactions of POMs with amino acids. Lately, our group prepared two novel 1D hetero-polymolybdates with copper−arg connectors $[Cu(arg)_2]_2[(CuO_6)Mo_6O_{18}(As_3O_3)_2]\cdot 4H_2O$ and $[Cu(arg)_2]_3[TeMo_6O_{24}]\cdot 8H_2O$ (arg = L-arginine).[97] Enlightened by the above results, we decided to explore the reactions of POMs with TM, Ln, and amino acid ligands. Nevertheless, the preparation of PTLHDs with amino acid ligands remains a rigorous challenge due to the following four main reasons: (i) it is well-known that the system containing TM, Ln, POMs, and organic components often results in immediate precipitation rather than crystallization;[31,32,36,38,42,98,99] (ii) highly negative charge PTLHDs are unfavorable to combine amino acid ligands; (iii) TM or Ln ions easily coordinate to the external O atoms of highly negative POMs in water solution, which renders combination of TM or Ln cations with amino acid ligands difficult; and (iv) the spatial hindrance of PTLHDs is unfavorable to integrating relatively large ligands. In this background, we have established a synthetic approach that permitted us to surmount these difficulties. On one hand, we selected the highly negative charge trivacant Keggin $[B\text{-}\alpha\text{-}SbW_9O_{33}]^{9-}$ polyoxoanion as the POM precursor to combine TM or Ln cations without forming precipitation. On the other hand, thr was opted as the ligand on account of its small size and flexibility (Scheme 1). In addition, for a reaction, initial

Scheme 1. Molecular Architecture of L-Threonine Ligand

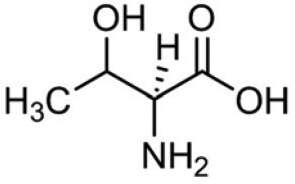

reactants, molar ratio, pH value, reaction time, temperature, etc. can often affect the formation of products. In the case of this work, some key points of preparing PTLHDs in water solution have been found. Lots of paralleling experiments indicate that initial reactants and the pH value are very important for the formation of the desired compounds. In order to deeply probe the influence of different TM ions on the structural architecture, we extended our studies to Mn^{2+}, Fe^{2+}, Co^{2+}, Ni^{2+}, and Zn^{2+} ions under similar conditions; only some amorphous phases were observed, which implied that the nature and chemical valence of TM ions played an important role in the construction of products.

IR Spectra. IR spectra of **1**−**7** are illustrated in Figure S1 of the Supporting Information, and all of them are very similar. In the low wavenumber domain (ν < 1000 cm^{-1}), characteristic vibrational bands originating from the trivacant Keggin $[B\text{-}\beta\text{-}SbW_9O_{33}]^{9-}$ framework, namely, $\nu(Sb-O_a)$, terminal $\nu(W-O_t)$, corner-sharing $\nu(W-O_b)$, and edge-sharing $\nu(W-O_c)$ are observed at 775−765, 952−945, 804−794, and 668−660 cm^{-1}, respectively. However, there is an apparent difference compared to the IR spectrum of $Na_{10}[B\text{-}\alpha\text{-}SbW_9O_{34}]\cdot 19.5H_2O$ [767, 920, 890, and 715 cm^{-1} for $\nu(Sb-O_a)$, $\nu(W-O_t)$, $\nu(W-O_b)$, and $\nu(W-O_c)$].[58] The shifts of $\nu(W-O_t)$, $\nu(Sb-O_a)$, $\nu(W-O_b)$, and $\nu(W-O_c)$ vibration frequencies are probably relevant to the embedding of the tetra-Fe^{III} $[Fe_4(H_2O)_8(thr)_2]^{12+}$ cluster to the defects of two $[B\text{-}\beta\text{-}SbW_9O_{33}]^{9-}$ as well as the transformation of $[B\text{-}\alpha\text{-}SbW_9O_{33}]^{9-} \rightarrow [B\text{-}\beta\text{-}SbW_9O_{33}]^{9-}$. However, the IR spectra of **1**−**7** were somewhat similar to that of the $[Sb_2W_{22}O_{74}(OH)_2]^{12-}$ polyanion,[58] owing to the fact that their polyoxoanionic skeletons are analogous, thus suggesting that the $[Fe_4(H_2O)_8(thr)_2(B\text{-}\beta\text{-}SbW_9O_{33})_2]^{6-}$ subunits of **1**−**7** still retain the basic Krebs' structure. The largish shifts or splitting in characteristic peaks may be caused by all internal and external tungsten atoms of the polyanion $[Sb_2W_{22}O_{74}(OH)_2]^{12-}$ replaced by four Fe^{3+} ions. Comparing with the IR spectrum of $[Fe_4(H_2O)_{10}(B\text{-}\beta\text{-}SbW_9O_{33})_2]^{6-}$ [948, 883, 807, 773, and 678 cm^{-1}],[48] characteristic vibration peaks of **1**−**7** have few shifts, which may be relevant to the grafting of two $[Ln(H_2O)_8]^{3+}$ ions to two terminals of $[Ln(H_2O)_8]_2[Fe_4(H_2O)_8(thr)_2(\beta\text{-}SbW_9O_{33})_2]$ subunits and the implanting of thr ligands to two external Fe^{3+} ions of $[Ln(H_2O)_8]_2[Fe_4(H_2O)_8(thr)_2(\beta\text{-}SbW_9O_{33})_2]$ subunits. In the IR spectra, the Ln−O stretching vibration is not observed perhaps due to the dominant ionic interactions between vacant POM fragments and Ln^{III} ions.[100] In the high-wavenumber region (ν > 1000 cm^{-1}), all compounds show a broad band at 3390−3408 cm^{-1} and a strong absorption band at 1625−1630 cm^{-1}, which are assigned to the stretching and bending vibrational modes of water molecules, respectively. But the $\nu(C{=}O)$ absorption bands of thr ligands are overlapped by the intense peaks of water ligands. Peaks at 1492−1501 cm^{-1} and 1393−1402 cm^{-1} are attributable to the $\nu(CH_3)$ vibrations. The peak at 1343−1354 cm^{-1} corresponds to the $\nu(C-N)$ vibration, while the signal at 1120−1144 cm^{-1} is indicative of the $\nu(C-O)$ vibrations. Generally, the coordination modes of the carboxylate (CO_2^-) group are anticipated to show very strong absorption peaks resulting from the asymmetric (1500−1650 cm^{-1}) and symmetric (1350−1460 cm^{-1}) stretching vibrations. The intense absorption peak at 1627−1630 cm^{-1} is ascribed to the $\nu(CO_2^-)$ asymmetric vibration [named as $\nu_{asym}(CO_2^-)$], while the absorption peak at 1393−1395 cm^{-1} is assigned to the $\nu(CO_2^-)$ symmetric vibration [named as $\nu_{sym}(CO_2^-)$]. Besides, the interval [$\Delta\nu = \nu_{asym}(CO_2^-) - \nu_{sym}(CO_2^-)$] between $\nu_{asym}(CO_2^-)$ and $\nu_{sym}(CO_2^-)$ has often been applied to judge the bonding modes of CO_2^- groups.[101,102] Generally speaking, if $\Delta\nu$ is greater than 200 cm^{-1}, CO_2^- groups utilize the monodentate fashion. In contrast, if $\Delta\nu$ is lower than 200 cm^{-1}, CO_2^- groups adopt the chelating mode. Thus, the $\Delta\nu$ of approximately 234−237

dx.doi.org/10.1021/cg5007988 | Cryst. Growth Des. 2014, 14, 6217−6229

cm^{-1} for **1**−**7** indicates the monodentate coordination fashion of CO_2^- groups of thr ligands.

Structural Description. Bond valence sum (BVS) calculations[103] of **1**−**7** demonstate that the chemical valences of all W, Fe, and Ln atoms are +6, +3, and +3, respectively (Table S1 of the Supporting Information). Specifically speaking, in **3**, the BVS values of W1, W2, W3, W4, W5, W6, W7, W8, W9, Fe1, Fe2, and Sm1 atoms are 6.15, 6.08, 6.04, 6.18, 6.17, 6.31, 6.22, 6.09, 5.91, 3.26, 3.28, and 3.31, respectively. In **4**, the BVS values of W1, W2, W3, W4, W5, W6, W7, W8, W9, Fe1, Fe2, and Eu1 atoms are 6.19, 5.94, 6.09, 6.10, 6.19, 6.20, 6.10, 6.06, 5.93, 3.17, 3.08, and 3.20, respectively. The XPS investigations on **3** and **4** were carried out to further affirm the chemical valences of W, Fe, and Ln atoms (Figure 1). The XPS spectra of **3** and **4** for W atoms

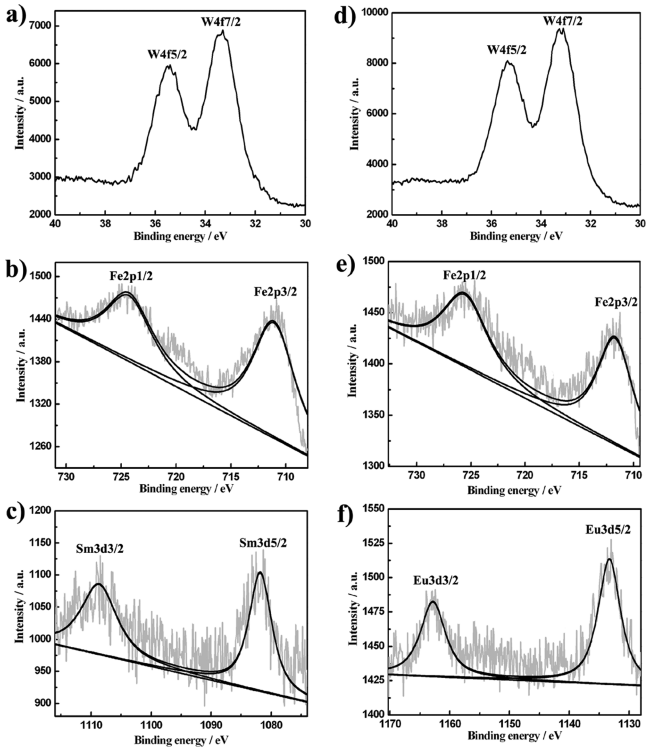

Figure 1. (a) The XPS pattern for W $4f_{7/2}$ and W $4f_{5/2}$ in **3**. (b) The XPS pattern for Fe $2p_{3/2}$ and Fe $2p_{1/2}$ in **3**. (c) The XPS pattern for Sm $3d_{5/2}$ and Sm $3d_{3/2}$ in **3**. (d) The XPS pattern for W $4f_{7/2}$ and W $4f_{5/2}$ in **4**. (e) The XPS pattern for Fe $2p_{3/2}$ and Fe $2p_{1/2}$ in **4**. (f) The XPS pattern for Eu $3d_{5/2}$ and Eu $3d_{3/2}$ in **4**.

display two signals with binding energies of 33.8 and 36.1 eV for **3**, 34.5 and 36.6 eV for **4**, attributing to W^{VI} ($4f_{7/2}$) and W^{VI} ($4f_{5/2}$), respectively. These results coincide with earlier reported values.[104,105] The Fe $2p_{1/2}$ and Fe $2p_{3/2}$ binding energies of 725.3 and 710.8 eV for **3** and 724.8 and 710.7 eV for **4** suggest the existence of the Fe^{III} centers in **3** and **4**.[106] Two peaks at 1081.8 and 1108.7 eV correspond to the Sm $3d_{5/2}$ and Sm $3d_{3/2}$ of the Sm^{III} cations in **3**.[107] As for **4**, two peaks at 1133.4 and 1163.1 eV are ascribed to the Eu $3d_{5/2}$ and Eu $3d_{3/2}$ of the Eu^{III} cations.[108] These are in good accordance with their BVS results.

1−**7** are isostructural and belong to the triclinic space group $P\bar{1}$, and their molecules consist of a $[Fe_4(H_2O)_8(thr)_2(B\text{-}\beta\text{-}SbW_9O_{33})_2]^{6-}$ with two supporting $[Ln(H_2O)_8]^{3+}$ cations on both sides, which represent the first organic−inorganic hybrid TAs containing $[B\text{-}\beta\text{-}SbW_9O_{33}]^{9-}$ subunits, TM cations, and Ln cations. Therefore, the structural description is exemplified by **1**. The molecular structure of **1** contains a neutral $[Pr(H_2O)_8]_2[Fe_4(H_2O)_8(thr)_2(B\text{-}\beta\text{-}SbW_9O_{33})_2]$ organic−inorganic hybrid unit and twenty-two crystallization water molecules (Figure 2a). It is worth pointing out that the

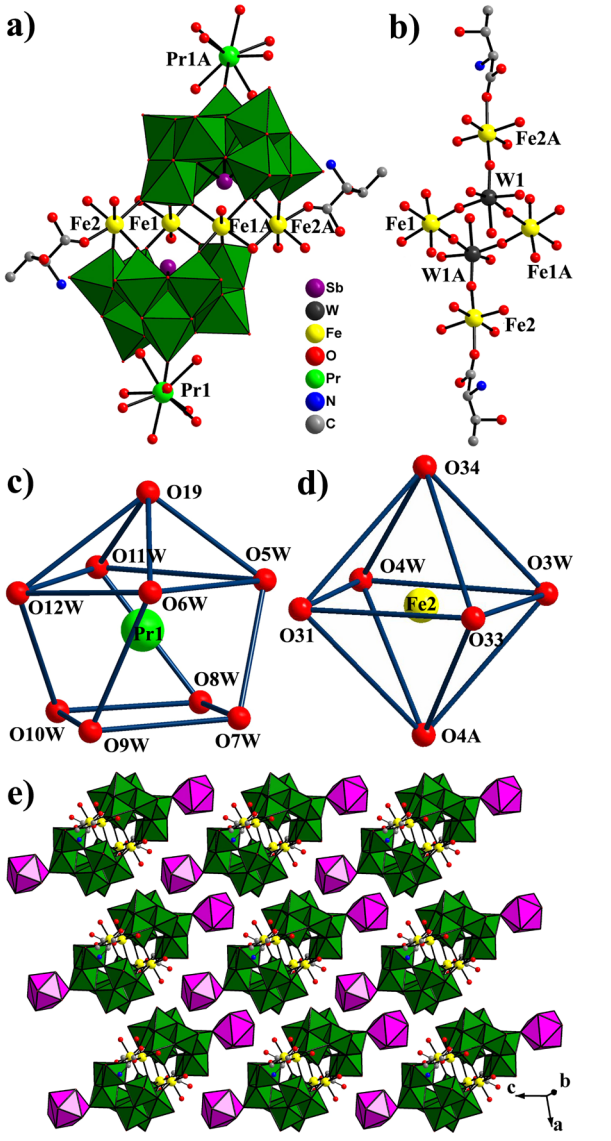

Figure 2. (a) The view of the molecule of **1** with the part labeling scheme. Crystallization waters are omitted for clarity. The atoms with the suffix A are generated by the symmetry operation where A: 1−*x*, 1−*y*, 1−*z*. (b) The connection between four Fe^{III} cations by two W^{VI} atoms in **1**. (c) The monocapped square antiprism environment of the $Pr1^{III}$ ion in **1**. (d) The octahedral environment of the $Fe2^{III}$ ions. (e) The regular alignment of discrete $[Pr(H_2O)_8]_2[Fe_4(H_2O)_8(thr)_2][B\text{-}\beta\text{-}SbW_9O_{33}]_2$ units.

$[Fe_4(H_2O)_8(thr)_2(B\text{-}\beta\text{-}SbW_9O_{33})_2]^{6-}$ subunit can be viewed as the result of two thr ligands substituting for two water ligands in the classical $[Fe_4(H_2O)_{10}(B\text{-}\beta\text{-}SbW_9O_{33})_2]^{6-}$ polyoxoanion (Figure 2, panels a and b). As far as we know, this phenomenon that two amino acid ligands substitute for two water ligands located on the sandwich belt of Krebs-type dimers is for the first time observed, although the replacement of two water ligands with two ox ligands was previously reported by Dolbecq et al.[51] Interestingly, the Pr^{III} cations grafting to the

dx.doi.org/10.1021/cg5007988 | Cryst. Growth Des. 2014, 14, 6217−6229

polyoxoanion inhabit in a nona-coordinate severely distorted monocapped square antiprism configuration (Figure 2c) defined by a terminal O atom from the trivacant Keggin [B-β-SbW_9O_{33}]$^{9-}$ fragment [Pr–O: 2.543(11) Å] and eight aqueous ligands [Pr1–O: 2.46(2)–2.59(3) Å]. The average of Pr–O bonds is 2.509 Å. Generally, the Ln^{III} cations mainly adopt seven-, eight-, or nine-coordinate geometries; however, this nine-coordinate monocapped square antiprism is rarely discovered in POM chemistry.[42,109] In the $[Fe_4(H_2O)_8(thr)_2(B\text{-}\beta\text{-}SbW_9O_{33})_2]^{6-}$ subunit, there are two types of inequivalent Fe^{3+} ions, namely, two inner Fe^{3+} ions (Fe1, Fe1A) and two outer Fe^{3+} ions (Fe2, Fe2A). Albeit two types of Fe^{3+} ions display the octahedral geometries (Figure 2d), their coordination environments are disparate. The octahedron of the Fe1 ion is established by two O atoms from one [B-β-SbW_9O_{33}]$^{9-}$ fragment [Fe–O: 1.940(9)–1.959(12) Å], two O atoms from the other [B-β-SbW_9O_{33}]$^{9-}$ fragment [Fe–O: 1.933(9)–1.955(13) Å], and two O atoms from two terminal H_2O molecules [Fe–O: 2.081(14)–2.106(13) Å], whereas the octahedral geometry of the Fe2 ion is constituted by two O atoms from one [B-β-SbW_9O_{33}]$^{9-}$ fragment [Fe–O: 1.930(14)–1.986(12) Å], one O atom from the other [B-β-SbW_9O_{33}]$^{9-}$ segment [Fe–O: 1.979(9) Å], two O atoms from two terminal H_2O molecules [Fe–O: 2.062(14)–2.072(15) Å], and a carboxyl O atom of thr ligand [Fe–O: 2.047(9) Å]. The four Fe atoms are situated on four vertexes of a rhombus with the neighboring two edge distances of 5.6355 and 5.6433 Å. Interestingly, four Fe^{3+} ions are separated by four Fe–O–W–O–Fe bonds (Figure 2b), and such a connection mode is somewhat distinct from those in the tetra-Fe^{III} substituted sandwich-type segments $[Fe_4(en)(\alpha\text{-}GeW_9O_{34})_2]^{8-}$ and $[Fe_4(en)_2(\alpha\text{-}GeW_9O_{34})_2]^{8-}$ reported by our group recently,[110] in which four iron centers are connected by Fe–O–Fe bonds.

Formally, the trivacant [B-β-SbW_9O_{33}]$^{9-}$ unit can be envisioned as originating from the parent β-Keggin anion by a removal of three edge-sharing $\{WO_6\}$ groups and is composed of three corner-sharing $\{W_3O_{13}\}$ trimers with a Sb^{3+} heteroatom connected by triply bridging O atoms and a 60° rotation of one $\{W_3O_{13}\}$ trimer. Considering that the [B-α-SbW_9O_{33}]$^{9-}$ subunit was used as the starting material in the process of the reaction, the occurrence of [B-β-SbW_9O_{33}]$^{9-}$ moiety in **1** indicates that the reaction process involves the B-α → B-β isomerization of the $[SbW_9O_{33}]^{9-}$ unit (Figure S2 of the Supporting Information). Such isomerization phenomenon has ever been observed in previous reports.[48,52,58,67] In the [B-β-SbW_9O_{33}]$^{9-}$ unit in **1**, seven O atoms (O_t) terminally bind to W atoms with W–O_t distances of 1.706(11)–1.735(10) Å; 13 O atoms (O_{w2}) link two W atoms with W–O_{w2} distances of 1.870(10)–2.043(12) Å; seven O atoms (O_{WFe}) being in conjunction with a W atom and a Fe atom have W–O_{WFe} distances of 1.772(10) to 1.844 (12) Å and Fe–O_{WFe} distances of 1.929(11) to 1.985 (11) Å; three O atoms (O_{w3Sb}) connect three W atoms and a Sb heteroatom and W–O_{w3Sb} distances are between 2.213(9) and 2.349(10) Å and Sb–O_{w3Sb} distances are 1.982(10)–2.004(9) Å.

The $[Fe_4(H_2O)_8(thr)_2(B\text{-}\beta\text{-}SbW_9O_{33})_2]^{6-}$ subunits in **1**–**7** are tightly relevant to $[Sb_2W_{22}O_{74}(OH)_2]^{12-}$ reported by Krebs and co-workers in 1997 that comprises two trilacunary Keggin-type [B-β-SbW_9O_{33}]$^{9-}$ segments connected through two internal $[WO_2]^{2+}$ and two external $[WO_2(OH)]^+$ groups (Figure 3a).[58] In 1999, Krebs et al. reported a similar Bi(III) species with the formula of $[Bi_2W_{22}O_{74}(OH)_2]^{12-}$.[111] Later, it was found that two outside $[WO_2(OH)]^+$ groups in these

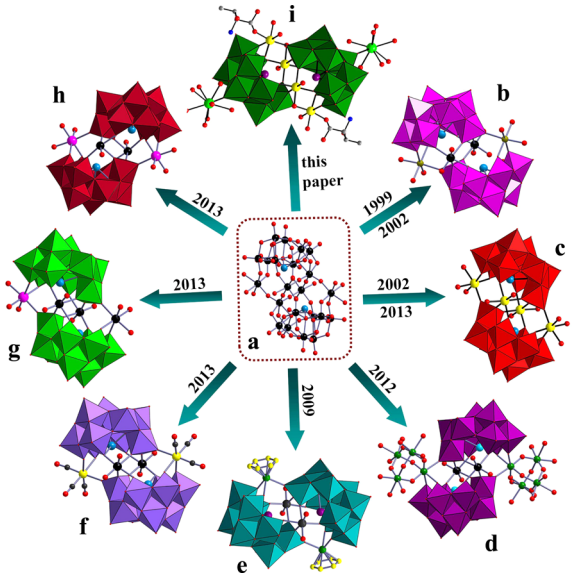

Figure 3. A summary of some typical Krebs dimeric POMs.

structure types can be replaced by various TM ions or main group metals, giving rise to the substituted Krebs dimers such as $[(WO_2)_2M_2(H_2O)_6(B\text{-}\beta\text{-}XW_9O_{33})_2]^{(14-2n)-}$ (X = Sb^{III}, Bi^{III}; M^{n+} = Mn^{2+}, Fe^{3+}, Co^{2+}, Ni^{2+}, VO^{2+}; X = Bi^{III}, M^{n+} = Fe^{3+}, Co^{2+}, Ni^{2+}, Cu^{2+}, and Zn^{2+}) (Figure 3b),[50,58,59,111,112] and $[(WO_2)_2(WO_2(OH))_{0.5}Sn_{1.5}(B\text{-}\beta\text{-}XW_9O_{33})_2]^{10.5-}$ (X = Sb^{III}, Bi^{III}).[113] Furthermore, internal $[WO_2]^{2+}$ and external $[WO_2(OH)]^+$ groups can also be replaced by main group metals or TMs forming $[M_4(H_2O)_{10}(\beta\text{-}XW_9O_{33})_2]^{n-}$ (X = As^{III}, Sb^{III}, Se^{IV}, Te^{IV}; M = Fe^{3+}, Mn^{2+}, Co^{2+}, Ni^{2+}, Cu^{2+}, Zn^{2+}, Cd^{2+}, Hg^{2+}, and In^{3+}; X = Sb^{III}, M = Al^{3+}) (Figure 3c).[48,59,114–117] More interestingly, Kortz et al. prepared two novel cubane $\{Ru_4O_6(H_2O)_9\}^{4+}$-substituted Krebs-type derivatives $[\{Ru^{IV}_4O_6(H_2O)_9\}_2Sb_2W_{20}O_{68}(OH)_2]^{4-}$ and $[\{Ru^{IV}_4O_6(H_2O)_9\}_2\{Fe(H_2O)_2\}_2\{\beta\text{-}TeW_9O_{33}\}_2H]^{-}$ (Figure 3d).[118] In addition, Kortz's group and Hill's group showed that two external tungsten centers can be substituted by organic metal cations in this structural type, and the typical examples are $[X_2W_{20}O_{70}(Ru^{II}L)_2]^{10-}$ (X = Sb^{III}, Bi^{III}) (L = benzene, p-cymene) (Figure 3e)[117] and $[X_2W_{20}O_{70}\{M(CO)_3\}_2]^{12-}$ (X = Sb^{III}, Bi^{III}; M = Re^{I}, Mn^{I}) (Figure 3f).[119] Very recently, Kortz et al. proved that external W^{VI} centers in this structure can be superseded by Ln ions, leading to $[Ln(H_2O)_4Sb_2W_{21}O_{72}(OH)]^{10-}$ (Ln = Yb^{III}, Lu^{III}) (Figure 3g) and $[Ln_2(H_2O)_8Sb_2W_{20}O_{70})]^{8-}$ (Ln = Yb^{III}, Lu^{III}, Y^{III}) (Figure 3h).[67] In this paper, seven Krebs dimeric POMs based on Sb_2W_{20} have been synthesized. Compared with the previous reports, the most obvious characteristics are observed in **1**–**7**: (a) amino acid ligands were successfully introduced to their structures through coordination of carboxyl O atoms of thr ligands to two external Fe^{III} centers in **1**–**7**; (b) Fe^{III} and Ln^{III} heterometal cations are simultaneously included in the structures and **1**–**7** represent the first organic–inorganic TA hybrids consisting of TM–Ln heterometal cations and amino acid components.

In addition, free $[Pr(H_2O)_8]_2[Fe_4(H_2O)_8(thr)_2][B\text{-}\beta\text{-}SbW_9O_{33}]_2$ units are regularly distributed (Figure 2e). From Figures 2e and 4, we can see that neighboring $[Pr(H_2O)_8]_2[Fe_4(H_2O)_8(thr)_2(B\text{-}\beta\text{-}SbW_9O_{33})_2]$ units are closely aligned in the staggered fashion, thus it can be concluded that a possible reason why the $[Pr(H_2O)_8]^{3+}$ cations selectively attach to the

dx.doi.org/10.1021/cg5007988 | Cryst. Growth Des. 2014, 14, 6217–6229

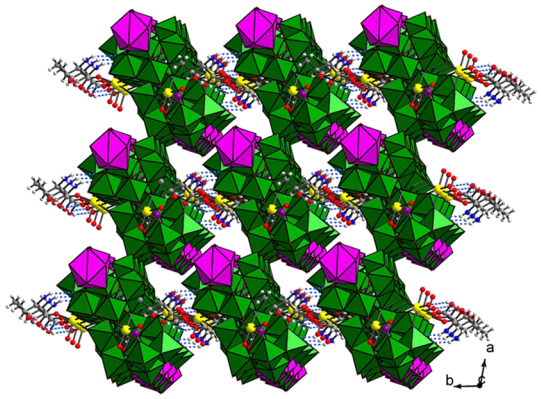

Figure 4. 3D supramolecular architecture of **1**. The light blue bonds highlight the hydrogen-bonding interactions.

O-sites on the "polar" position of the $[B\text{-}\beta\text{-}SbW_9O_{33}]^{9-}$ group is that the grafting of the $[Pr(H_2O)_8]^{3+}$ cations to the O-sites on both "polar" positions of $[Fe_4(H_2O)_8(thr)_2(B\text{-}\beta\text{-}SbW_9O_{33})_2]^{6-}$ are able to effectively decrease the steric hindrance and favors the closest packing of $[Pr(H_2O)_8]_2[Fe_4(H_2O)_8(thr)_2(B\text{-}\beta\text{-}SbW_9O_{33})_2]$ units. It is worth mentioning that the design and construction of metal-involved supramolecular networks have attracted increasing attention in the field of crystal engineering and supramolecule chemistry since they can provide novel topologies and new materials.[120,121] Moreover, POM-based supramolecular compounds are one of the most prospective candidates in the field of chemicobiology, material chemistry, etc.[122−124] In this respect, the 3D supramolecular structure also exists in **1**. For each thr ligand, only one carboxylic O atoms participate in coordination, and it can form O−H···O interactions with both coordinated and lattice water molecules. What is more, the N atoms of thr ligands can form hydrogen-bonding interactions with the O atoms of the POMs and water molecules. As a result, it can be seen that thr ligands are proton donors and surface O atoms of $[B\text{-}\beta\text{-}SbW_9O_{33}]^{9-}$ fragments and water molecules are proton acceptors. Combined actions between donors and acceptors give rise to the 3D supramolecular structure (Figure 4) with N−H···O distances of 3.00(5)−3.18(3) Å and O−H···O distances of 2.68(3)−3.08(3) Å. These hydrogen bonds may further enhance cohesion of the structures.

Photoluminescence Properties. It is well-known that lanthanoid complexes exhibit attractive luminescent performances and can be applied in diverse domains, including lasers, optical devices, sensory probes, and so on,[125] which are chiefly related to the fact that the 4f electrons are shielded by the outer 5s and 5p electrons resulting in well-defined absorption and emission bands.[126] Consequently, the atomic properties of lanthanoid ions are usually maintained in the complexes. Emission band derived from the oxygen-to-metal (O → M) transitions of POM units are able to generate intramolecular energy transport from the O → M excited states to the Ln^{III} excited energy levels, and then to sensitize the Ln emission. Since the intramolecular energy transfer from POMs to Ln cations can occur by means of ligand-to-metal charge transfer (LMCT), the luminescent properties of some POM-based Ln derivatives were studied by Yamase and other research groups.[127,128] Thereby, the emission behavior of **4** has been measured at room temperature (the excitation spectrum monitored at 615 nm of **4** is displayed in Figure S3 of the Supporting Information). The solid-state emission spectrum of **4** under excitation at 310 nm display five emission peaks of the Eu^{III} ions, which are associated with $^5D_0 \rightarrow {}^7F_J$ (J = 0, 1, 2, 3, 4) [$^5D_0 \rightarrow {}^7F_0$ (564 nm), $^5D_0 \rightarrow {}^7F_1$ (594 nm), $^5D_0 \rightarrow {}^7F_2$ (618 nm), $^5D_0 \rightarrow {}^7F_3$ (648 nm), and $^5D_0 \rightarrow {}^7F_4$ (700 nm)] transitions (Figure 5a). As we know, the $^5D_0 \rightarrow {}^7F_0$ transition is

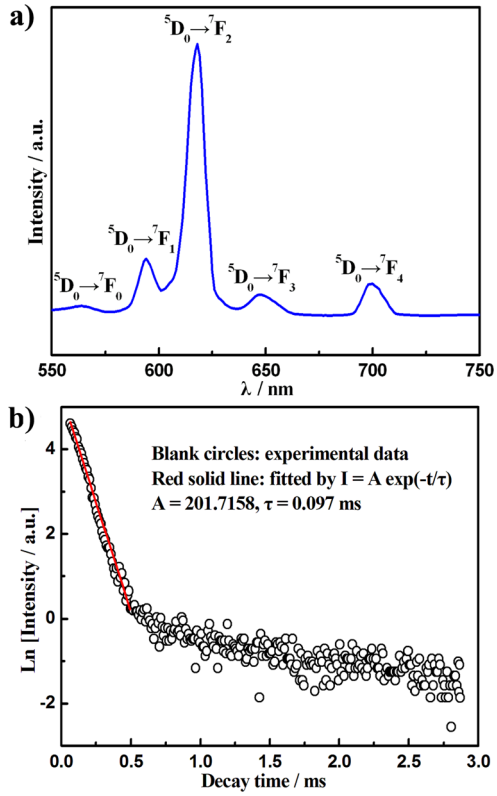

Figure 5. (a) The emission spectrum of **4** under excitation at 310 nm at room temperature. (b) The luminescence decay curve of **4**.

severely forbidden in a symmetric field. However, the weak $^5D_0 \rightarrow {}^7F_0$ emission at 564 nm can still be observed in **4**, revealing that the Eu^{III} ions are located in the lower symmetric ligand field, which is in good agreement with the monocapped square antiprism of the Eu^{III} ions. Furthermore, the $^5D_0 \rightarrow {}^7F_0$ transition exhibits the single band in **4**, suggesting one local site-symmetric chemical environment of the Eu^{III} ions. The magnetic-dipolar $^5D_0 \rightarrow {}^7F_{1,3}$ transitions lack sensitivity to the local microenvironments, whereas the electric-dipolar $^5D_0 \rightarrow {}^7F_{2,4}$ transitions are highly sensitive to the local microenvironments.[129] Generally speaking, the emission intensity of the magnetic dipole $^5D_0 \rightarrow {}^7F_1$ transitions scarcely changes with the strength of ligand field exerting on Eu^{III} ions, whereas the intensity of the electric dipole $^5D_0 \rightarrow {}^7F_2$ transitions is highly sensitive to the chemical bonds in the neighborhood of Eu^{III} ions. The $^5D_0 \rightarrow {}^7F_1$ transitions are dominating in a centrosymmetric environment while the $^5D_0 \rightarrow {}^7F_2$ transition becomes the strongest in a noncentrosymmetric situation.[130,131] The $^5D_0 \rightarrow {}^7F_2$ intensity rises with the decrease of the site symmetry of Eu^{III} ions. As a consequence, the intensity ratio of the $^5D_0 \rightarrow {}^7F_2/{}^5D_0 \rightarrow {}^7F_1$ transitions is generally served as checking the local chemical circumstances of the Eu^{III} cations and is functioned as a criterion of the site symmetry of the Eu^{III} ions.[132] The intensity ratio in **4** is 4.7, reflecting the low site symmetry of the Eu^{III} ions, which is in good consistence with the distorted monocapped square antiprism geometry of Eu^{III}

dx.doi.org/10.1021/cg5007988 | Cryst. Growth Des. 2014, 14, 6217−6229

cations. In addition, to further determine lifetime, the semilogarithmic plot of the luminescent decay curve of **4** has also been carried out (Figure 5b). The semilogarithmic plot for ln[Intensity] versus decay time can be fitted to the single exponential function $[I = A \exp(-t/\tau)]$ and the lifetime τ is 0.097 ms. The decay time for **4** is shorter than those for $K_{13}[Eu(SiW_{11}O_{39})_2]$ (2.440 ms) and $Na_{0.5}Cs_{4.5}[Eu(\alpha\text{-}SiW_{11}O_{39})(H_2O)_2]\cdot 23H_2O$ (0.39 ms),[133] mainly because water ligands on Ln cations can enhance the radiationless deactivation of the $^5D_0$ state and partly quench the luminescence emission.[133] Obviously, eight water molecules are bonded to the Eu^{3+} ion in **4**; the Eu^{3+} cation in $K_{13}[Eu(SiW_{11}O_{39})_2]$ is defined by eight oxygen atoms of two $[\alpha\text{-}SiW_{11}O_{39}]^{8-}$ fragments, and the Eu^{3+} cation is coordinated by two water ligands in $Na_{0.5}Cs_{4.5}[Eu(\alpha\text{-}SiW_{11}O_{39})(H_2O)_2]\cdot 23H_2O$; therefore, the shorter decay time for **4** can be expected.

Electrochemical and Electrocatalytic Properties. Over the past dozens of years, considerable interest has been focused on the electrochemical studies of heteropolyanions and especially their metal-substituted derivatives, partly because of their possible applications in electrocatalysis and chemically modified-electrode field.[134−137] In this context, multifarious POM-based modified electrodes were developed.[138−140] Interestingly, although **1** was prepared in conventional aqueous solution, the solubility in water was very low, therefore, taking advantage of cyclic voltammetry, we investigated the solid-state electrochemistry and electrocatalytic performances of **1** in a 0.5 mol L^{-1} Na_2SO_4+H_2SO_4 medium by the modified CPE. The cyclic voltammogram (CV) of **1** in pH 1.91 sulfate medium at the scan speed of 50 mV s^{-1} is illustrated in Figure 6a at room temperature. It can be seen that four groups of redox peaks are observed between −1.0 and 1.0 V, and their midpoint potentials are −0.693 V (I−I′), −0.407 V (II−II′), 0.166 V (III−III′), and 0.445 V (VI−VI′) (the reference electrode is Ag/AgCl), respectively. Obviously, the redox peaks of W^{VI} centers fragments appear at a more negative potential region than that assigned to the Fe^{III} centers. The I−I′, II−II′, and III−III′ redox peaks in the CV of **1** are attributed to the oxidation−reduction procedure of the W^{VI} centers in the TA fragments.[138,141] The peak at 0.445 V is identified as the oxidation−reduction process of the Fe^{III} centers.[48,142−144] Besides, the effect of scan rate (ν) on the electrochemistry of **1**-CPE was explored in the aforementioned conditions. Figure 6b exhibits the evolution of the cathodic and anodic currents of the W^{VI}-based wave with different scan rates, it can clearly be seen that with elevating scan rates from 80 to 320 mV s^{-1}, the cathodic peak potentials move to the negative orientation, while the corresponding anodic peak potentials proceed toward the positive orientation. Though the peak potential differences between the corresponding cathodic and anodic waves increase, the midpoint potential hardly moves. The increase of the peak potential differences with increasing scan rate are related to the fact that protons coming from solution diffuse into **1**-CPE to maintain the charge balance when **1**-CPE is reduced, thus the diffusion speed of protons into **1**-CPE starts to decide the electrochemical reduction speed as the increase of the scan speed.[145] When the scan speed varies between 80 and 320 mV s^{-1}, the relationship between the peak current (I_{pc}) and the scan speed is linear (Figure 6c), and its linear function is $I_{pc} = -0.00016\nu - 0.03200$ with the consistency factor of 0.99386, which reveals that the redox process of **1**-CPE is surface-controlled.[44,140]

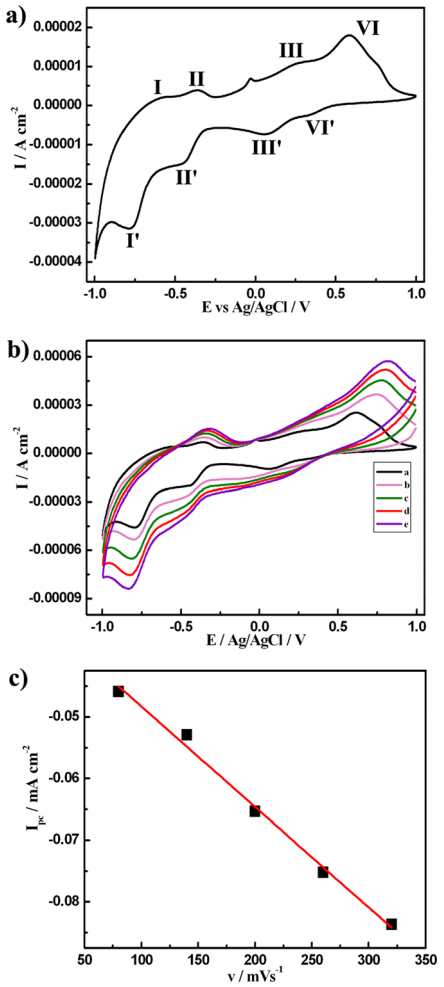

Figure 6. (a) The CV of **1**-CPE in pH = 1.91 0.5 mol L^{-1} Na_2SO_4 + H_2SO_4 aqueous solution. Scan speed: 80 mV s^{-1}. (b) CVs of **1**-CPE at variable scan speeds (a, 80; b, 140; c, 200; d, 260; e, 320 mV s^{-1}). (c) The linear relationship between cathodic peak currents (I′) and the scan speed for **1**-CPE.

Recently, the efficient electrocatalytic reduction of POMs is an area of continuing interest for the sake of their faculty to experience rapid reversible multiple electron-transfer procedures. Some promising results were reported, which exhibited that POMs can transmit electrons to other species. For example, Kortz et al. demonstrated the remarkable electrocatalytic efficiency for the nitrite, nitric oxide, and nitrate reduction reaction of $[Fe_6(OH)_3(A\text{-}\alpha\text{-}GeW_9O_{34}(OH)_3)_2]^{11-}$.[146] Wang and co-workers indicated that two novel high-nuclear copper-substituted POMs $Na_{16}[Cu_{14}(OH)_4(H_2O)_{16}(SiW_8O_{31})_4]\cdot 20.5H_2O$ and $K_{10}Na_{14}[Cu_{10}(H_2O)_2(N_3)_4(GeW_9O_{34})_2(GeW_8O_{31})_2]\cdot 30H_2O$ can act as catalysts during the course of the nitrate reduction.[137] Mbomekalle and Dolbecq suggest that the mixed Fe−Ni-substituted Dawson POM $[Ni_2(H_2O)_2Fe_2(As_2W_{15}O_{56})_2]^{14-}$ can undergo multielectron redox processes and shows the efficient activity to the reduction of NO_2^-, O_2, and H_2O_2.[147] Hill et al. compared the electrocatalytic performances toward the reduction of H_2O_2, O_2, and NO_2^- for two mixed metal substituted sandwich-type POMs $Ni_2Fe_2P_4$ and $Ni_2Fe_2As_4$.[148] Very recently, our group has explored the electrocatalytic activities of two Cu^{II}−Ln^{III} heterometallic germanotungstates toward nitrite and bromate reduction.[44,45]

dx.doi.org/10.1021/cg5007988 | Cryst. Growth Des. 2014, 14, 6217−6229

Here, **1**-CPE was applied to investigate the electrocatalytic reduction of BrO_3^- and H_2O_2 in 0.5 mol L^{-1} sulfate medium (pH = 1.51). As we know, bromate exists in potable water as a subsidiary product of an ozone sterilizing agent and is usually served as a food additive. Furthermore, people have a suspicion that bromate is a human carcinogen and, as a result, monitoring or removing this species is interesting from the viewpoint of human health.[149−151] As a rule, the bromate reduction is entirely nonreversible at a glassy carbon electrode in acidic water medium and does not occur in preference to the evolution of hydrogen.[138] To evaluate the electrocatalytic activity of **1**-CPE to the BrO_3^- reduction, the variation of CVs of **1**-CPE in the 0.5 mol L^{-1} acidic sulfate medium with the amount of different $NaBrO_3$ have been recorded at room temperature. From Figure 7a, it can clearly be observed that the

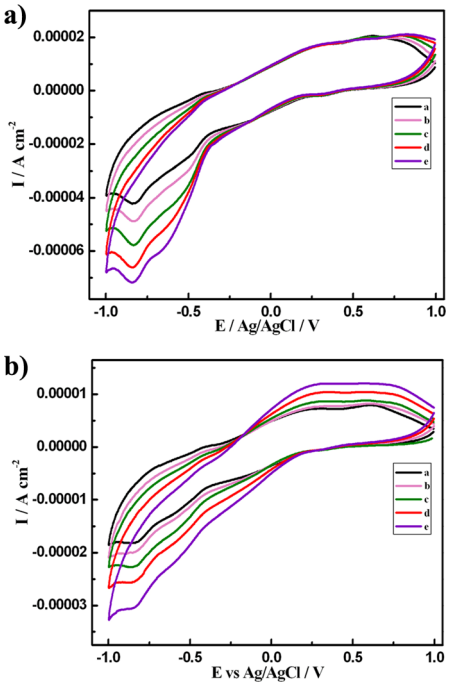

Figure 7. (a) The variation of CVs of **1**-CPE in pH = 1.91 0.5 mol L^{-1} Na_2SO_4 + H_2SO_4 aqueous solution with the amount of different $NaBrO_3$ (a, 3×10^{-3}; b, 7×10^{-3}; c, 1.1×10^{-2}; d, 1.5×10^{-2}; e, 1.9×10^{-2} mol L^{-1}). (b) The variation of CVs of **1**-CPE in pH = 1.91 0.5 mol L^{-1} Na_2SO_4 + H_2SO_4 aqueous solution with the amount of different H_2O_2 (a, 5.88×10^{-3}; b, 1.37×10^{-2}; c, 2.16×10^{-2}; d, 2.94×10^{-2}; e, 3.72×10^{-2} mol L^{-1}). Scan speed: 80 mV s^{-1}.

cathodic reduction current intensity of the W^{VI} centers gradually increases with the addition of $NaBrO_3$; in the meantime, the opposite oxidation peak current intensity gradually declines. However, the Fe^{III}-based reduction peak intensity is almost uninfluenced with the addition of bromate. This result suggests that **1**-CPE exhibits the remarkable electrocatalytic activity to the BrO_3^- reduction, and the reduction of BrO_3^- is chiefly controlled by the W-based wave in **1**. In fact, similar results have been previously encountered by us.[44,45] As far as we know, improving electrocatalytic activity of H_2O_2 is interesting for application fields in biosensors, fuel cells, etc.[152] To date, numerous POMs have previously been exploited for the reduction of hydrogen peroxide.[137,147,153] In this paper, **1**-CPE is also evaluated for the electrocatalytic reduction of hydrogen peroxide. From Figure 7b, we can find that upon adding H_2O_2, the reduction peak current of W^{VI}-based wave rises and the corresponding oxidation peak current wanes; meanwhile, in the positive potential domain the Fe^{III}-based peak current intensity changes, which significantly differs from the BrO_3^- electrocatalytic reduction. These results reveal that the H_2O_2 electrocatalytic reduction is simultaneously mediated by the reduced species of the W^{VI}-based and Fe^{III}-based waves in **1**-CPE.

Magnetic Properties. Recently, magnetic heterometallic TM−Ln compounds in coordination chemistry and materials science have drawn considerable attention.[154−156] Hitherto, although various heterometallic TM−Ln compounds have been obtained, apart from the f^7 Gd^{3+} ion and the orbital nondegenerate ground state, there is little knowledge about the essence and magnitude of the magnetic couplings of Ln ions between themselves and other TM centers,[157] which is essentially relevant to the case that magnetisms of most Ln ions are powerfully affected by spin−orbit coupling that entails it to be difficult for quantitatively interpreting magnetic interactions.[17,158,159] Generally, in comparison with TM ions, Ln ions have more significant orbital contribution of the magnetic moment; as a result, the ligand field effect is smaller and spin−orbit coupling is larger for the Ln ions.[69] Interelectronic repulsion and spin−orbit coupling usually entail the ^{2S+1}L term of one Ln ion to split into $^{2S+1}L_J$ spectroscopic levels,[157,160] and then the crystal field perturbation makes each $^{2S+1}L_J$ level further split into Stark sublevels. Though the magnetic theory of Ln ions has been known for a long time, the large unquenched orbital angular momentum contribution hinders people from developing the simple models to reasonably analyze the correlation between structure and magnetism.[160] Herein, magnetic properties for **3** and **6** were measured on the polycrystalline samples in 1.8−300 K under a 100 Oe applied field. Their plots of χ_M, $\chi_M T$ versus T are illustrated in Figure 8 (panels a−d).

For **3**, the χ_M displays a gradual rise from 0.067 emu mol^{-1} at 300 K to 0.34 emu mol^{-1} at 50 K and fleetly arrives at the maximum of 4.17 emu mol^{-1} at 1.8 K (Figure 8a). Correspondingly, the $\chi_M T$ of 20.16 emu K mol^{-1} at 300 K is obviously greater than the theoretical value of 17.68 emu K mol^{-1} calculated for four isolated Fe^{3+} cations ($S = 5/2$, $g = 2$) and two noninteracting Sm^{3+} cations ($^6H_{5/2}$, $J = 5/2$, $g = 2/7$).[161] Upon cooling, the $\chi_M T$ decreases gradually to 7.46 emu K mol^{-1} at 1.8 K, which is mainly due to the depopulation of the Kramers doublets of higher energy of the Sm^{3+} ion. Generally, the ^6H ground term of the Sm^{3+} cation in the ligand field is split into six states ($J = 5/2$, 7/2, 9/2, 11/2, 13/2, and 15/2) by spin−orbit coupling, which usually results in the thermal population of some high-energy states (for example, the first excited states $^6H_{7/2}$ and ever higher excited states) at room temperature. Similar phenomena were discovered in Sm^{III}-containing complexes $[\{Sm(H_2O)_6\}_2As_8V_{14}O_{42}(SO_3)]\cdot 8H_2O$[161] and $[Sm(hfac)_3(NIT\text{-}5\text{-}Br\text{-}3py)]_2$.[162] The curve of χ_M^{-1} versus temperature obeys the Curie−Weiss equation, affording $C = 21.00$ emu K mol^{-1} and $\theta = -8.08$ K (Figure 8b). The small θ value is indicative of the weak effect of the ligand field in **3**.

With respect to **6**, the $\chi_M T$ at 300 K is 48.16 emu K mol^{-1}, being slightly larger than the theoretical value (45.84 emu K mol^{-1}) for four free Fe^{3+} cations ($S = 5/2$, $g = 2$) and two isolated Dy^{3+} cations ($^6H_{15/2}$, $J = 15/2$, $g = 4/3$).[163,164] The $\chi_M T$ reaches to the greatest value of 63.86 emu K mol^{-1} at 70 K during the cooling period (Figure 8c). This profile may

dx.doi.org/10.1021/cg5007988 | Cryst. Growth Des. 2014, 14, 6217−6229

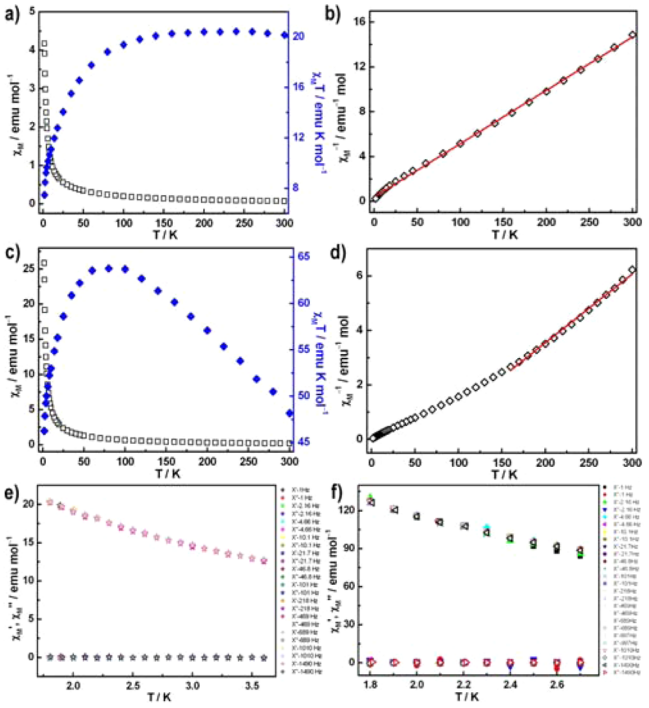

Figure 8. (a) The plots of χ_M, $\chi_M T$ versus T for **3** between 2 and 300 K. (b) The plot of χ_M^{-1} versus T for **3** between 2 and 300 K. (c) The plots of χ_M, $\chi_M T$ versus T for **6** between 2 and 300 K. (d) The plot of χ_M^{-1} versus T for **6** between 2 and 300 K. The red line is generated by the Curie–Weiss law. (e) Variable-temperature in-phase (χ_M') and out-of-phase (χ_M'') alternating current susceptibilities at various frequencies for **3** under zero Oe direct current field. (f) Variable-temperature in-phase (χ_M') and out-of-phase (χ_M'') alternating current susceptibilities at various frequencies for **3** under zero Oe direct current field.

manifest that the S_{Fe} = 5/2 or S_{Dy}= 9/2 local spins to some extent are liable to align along the same direction.[165] Such phenomenon has been observed by us.[7] $\chi_M T$ undergoes a sudden drop as temperature is lowered from 70 to 1.8 K, which can be assigned to the intermolecular antiferromagnetic interactions.[166,167] What is more, the magnetic data between 160 and 300 K can be described by the Curie–Weiss law resulting in C = 39.61 emu K mol^{-1} and θ = 59.78 K (Figure 8d), which can to some extent confirm the presence of the ferromagnetic couplings resulting from the parallel of local spins. To investigate whether the magnetic coupling can lead to the SMM behavior, the alternating current magnetic susceptibility measurements of **3** and **6** were performed (Figure 8 (panels e and f). The in-phase (χ_M') and out-of-phase (χ_M'') signals at low temperatures of **3** and **6** do not exhibit frequency dependence with an increase of the frequency, clearly illustrating the lack of slow magnetization relaxation in **3** and **6**, which may originate from fast quantum tunneling and/or the absence of low population excited levels.[168]

CONCLUSIONS

In conclusion, a series of Fe^{III}–Ln^{III} heterometallic trilacunary Keggin TAs **1**–**7** has been successfully prepared in conventional water solution and structurally characterized. X-ray diffraction structural analyses indicate that isomorphic **1**–**7** are constructed from a $[Fe_4(H_2O)_8(thr)_2(B\text{-}\beta\text{-}SbW_9O_{33})_2]^{6-}$ subunit with two supporting $[Ln(H_2O)_8]^{3+}$ cations on both sides. For all we know, **1**–**7** represents the unique TM–Ln heterometallic TA hybrids consisting of amino acid components. The luminescence properties of **4** have been probed. Furthermore, the electrochemistry of **1** has been performed in Na_2SO_4+H_2SO_4 medium by the modified electrode technique. **1**-CPE manifests the obvious activity to the electrocatalytic reduction of BrO_3^- and H_2O_2. Variable temperature susceptibility data for **3** and **6** were measured. **3** and **6** do not display the slow magnetization relaxation, which are likely to have relation with fast quantum tunneling and/or be short of low-lying excited levels. These findings open up a door for exploring TM–Ln heterometallic TAs. The following work will be devoted to manufacture novel POM-based functional materials through implanting polycarboxylic or chiral ligands to this reaction system.

ASSOCIATED CONTENT

Supporting Information

Comparison of reaction conditions and related phases involving $[B\text{-}\alpha\text{-}SbW_9O_{33}]^{9-}$ and TM or Ln cations, BVS calculations of all W, Fe, and Ln atoms in **1**–**7**; IR spectra and related structural figures; the excitation spectrum of **4**; and crystal data in CIF format. Crystal data have been deposited at the Cambridge Crystallographic Data Center, CCDC 1005844–1005850 for **1**–**7**. This material is available free of charge via the Internet at http://pubs.acs.org.

AUTHOR INFORMATION

Corresponding Authors

*E-mail: zhaojunwei@henu.edu.cn. Fax: (+86) 371 23886876.
*E-mail: ljchen@henu.edu.cn.

Notes

The authors declare no competing financial interest.

ACKNOWLEDGMENTS

We are thankful for the NSFC (Grants 21101055, 21301049, and U1304208), the Natural Science Foundation of Henan Province (Grants 122300410106 and 102300410093), the Foundation of State Key Laboratory of Structural Chemistry (Grant 20120013), the 2014 Special Foundation for Scientific Research Project of Henan University, the 2012 Young Backbone Teachers Foundation from Henan Province, and the Students Innovative Pilot Plan of Henan University (2013, 2014).

REFERENCES

(1) Bassil, B. S.; Ibrahim, M.; Al-Oweini, R.; Asano, M.; Wang, Z. X.; Tol, J. V.; Dalal, N. S.; Choi, K. Y.; Biboum, R. N.; Keita, B.; Nadjo, L.; Kortz, U. *Angew. Chem., Int. Ed.* **2011**, *50*, 5961–5964.
(2) Mal, S. S.; Kortz, U. *Angew. Chem., Int. Ed.* **2005**, *44*, 3777–3780.
(3) Ritchie, C.; Ferguson, A.; Nojiri, H.; Miras, H. N.; Song, Y. F.; Long, D. L.; Burkholder, E.; Murrie, M.; Kögerler, P.; Brechin, E. K.; Cronin, L. *Angew. Chem., Int. Ed.* **2008**, *47*, 5609–5612.
(4) Sadakane, M.; Steckhan, E. *Chem. Rev.* **1998**, *98*, 219–238.
(5) Pardo, R.; Zayat, M.; Levy, D. *Chem. Soc. Rev.* **2011**, *40*, 672–687.
(6) Mitchell, S. G.; Streb, C.; Miras, H. N.; Boyd, T.; Long, D. L.; Cronin, L. *Nat. Chem.* **2010**, *2*, 308–312.
(7) Rhule, J. T.; Hill, C. L.; Judd, D. A. *Chem. Rev.* **1998**, *98*, 327–357.
(8) Long, D. L.; Tsunashima, R.; Cronin, L. *Angew. Chem., Int. Ed.* **2010**, *49*, 1736–1758.
(9) Zhou, J.; Zhao, J.-W.; Wei, Q.; Zhang, J.; Yang, G.-Y. *J. Am. Chem. Soc.* **2014**, *136*, 5065–5071.

(10) Winter, R. S.; Yan, J.; Busche, C.; Mathieson, J. S.; Prescimone, A.; Brechin, E. K.; Long, D. L.; Cronin, L. *Chem.—Eur. J.* **2013**, *19*, 2976−2981.
(11) Huang, L.; Zhang, J.; Cheng, L.; Yang, G. Y. *Chem. Commun.* **2012**, *48*, 9658−9660.
(12) Huang, L.; Cheng, L.; Fang, W.-H.; Wang, S.-S.; Yang, G. Y. *Eur. J. Inorg. Chem.* **2013**, 1639−1643.
(13) Li, X.-X.; Zheng, S. T.; Zhang, J.; Fang, W. H.; Yang, G. Y.; Clemente-Juan, J. M. *Chem.—Eur. J.* **2011**, *17*, 13032−13043.
(14) Zheng, S. T.; Zhang, J.; Li, X. X.; Fang, W. H.; Yang, G. Y. *J. Am. Chem. Soc.* **2010**, *132*, 15102−15103.
(15) Zheng, S. T.; Zhang, J.; Clemente-Juan, J. M.; Yuan, D. Q.; Yang, G. Y. *Angew. Chem., Int. Ed.* **2009**, *121*, 7312−7315.
(16) Zhang, S. W.; Zhang, D. D.; Ma, P. T.; Liang, Y. F.; Wang, J. P.; Niu, J. Y. *CrystEngComm* **2013**, *15*, 2992−2998.
(17) Zhang, S. W.; Wang, Y.; Zhao, J. W.; Ma, P. T.; Wang, J. P.; Niu, J. Y. *Dalton Trans.* **2012**, *41*, 3764−3772.
(18) Li, F. Y.; Guo, W. H.; Xu, L.; Ma, L. F.; Wang, Y. C. *Dalton Trans.* **2012**, *41*, 9220−9226.
(19) An, H. Y.; Zhang, H.; Chen, Z. F.; Li, Y. G.; Liu, X.; Chen, H. *Dalton Trans.* **2012**, *41*, 8390−8400.
(20) Andruh, M.; Costes, J. P.; Diaz, C.; Gao, S. *Inorg. Chem.* **2009**, *48*, 3342−3359.
(21) Reinoso, S. *Dalton Trans.* **2011**, *40*, 6610−6615.
(22) Feng, X. J.; Zhou, W. Z.; Li, Y. G.; Ke, H. S.; Tang, J. K.; Clérac, R.; Wang, Y. H.; Su, Z. M.; Wang, E. B. *Inorg. Chem.* **2012**, *51*, 2722−2724.
(23) Chen, W. L.; Li, Y. G.; Wang, Y. H.; Wang, E. B.; Zhang, Z. M. *Dalton Trans.* **2008**, 865−867.
(24) Xue, G. L.; Liu, B.; Hu, H. M.; Yang, J. H.; Wang, J. W.; Fu, F. *J. Mol. Struct.* **2004**, *690*, 95−103.
(25) Fang, X. K.; Koegerler, P. *Chem. Commun.* **2008**, 3396−3398.
(26) Fang, X. K.; Kögerler, P. *Angew. Chem., Int. Ed.* **2008**, *47*, 8123−8126.
(27) Chen, W. L.; Li, Y. G.; Wang, Y. H.; Wang, E. B. *Eur. J. Inorg. Chem.* **2007**, 2216−2220.
(28) Yao, S.; Zhang, Z. M.; Li, Y. G.; Lu, Y.; Wang, E. B.; Su, Z. M. *Cryst. Growth Des.* **2010**, *10*, 135−139.
(29) Li, Y. W.; Li, Y. G.; Wang, Y. H.; Feng, X. J.; Lu, Y.; Wang, E. B. *Inorg. Chem.* **2009**, *48*, 6452−6458.
(30) Zhang, Z. M.; Li, Y. G.; Yao, S.; Wang, E. B. *Dalton Trans.* **2011**, *40*, 6475−6479.
(31) Nohra, B.; Mialane, P.; Dolbecq, A.; Rivière, E.; Marrot, J.; Sècheresse, F. *Chem. Commun.* **2009**, 2703−2705.
(32) Compain, J.-D.; Mialane, P.; Dolbecq, A.; Mbomekallé, I. M.; Marrot, J.; Sécheresse, F.; Duboc, C.; Rivière, E. *Inorg. Chem.* **2010**, *49*, 2851−2858.
(33) Reinoso, S.; Galán-Mascarós, J. R. *Inorg. Chem.* **2010**, *49*, 377−379.
(34) Reinoso, S.; Galán-Mascarós, J. R.; Lezama, L. *Inorg. Chem.* **2011**, *50*, 9587−9593.
(35) Ismail, A. H.; Bassil, B. S.; Yassin, G. H.; Keita, B.; Kortz, U. *Chem.—Eur. J.* **2012**, *18*, 6163−6166.
(36) Zhao, H. Y.; Zhao, J. W.; Yang, B. F.; He, H.; Yang, G. Y. *CrystEngComm* **2013**, *15*, 5209−5213.
(37) Zhao, H. Y.; Zhao, J. W.; Yang, B. F.; He, H.; Yang, G. Y. *CrystEngComm* **2013**, *15*, 8186−8194.
(38) Niu, J. Y.; Zhang, S. W.; Chen, H. N.; Zhao, J. W.; Ma, P. T.; Wang, J. P. *Cryst. Growth Des.* **2011**, *11*, 3769−3777.
(39) Zhao, J. W.; Shi, D. Y.; Chen, L. J.; Li, Y. Z.; Ma, P. T.; Wang, J. P.; Niu, J. Y. *Dalton Trans.* **2012**, *41*, 10740−10751.
(40) Shi, D. Y.; Zhao, J. W.; Chen, L. J.; Ma, P. T.; Wang, J. P.; Niu, J. Y. *CrystEngComm* **2012**, *14*, 3108−3119.
(41) Zhang, S. W.; Zhao, J. W.; Ma, P. T.; Niu, J. Y.; Wang, J. P. *Chem.—Asian J.* **2012**, *7*, 966−974.
(42) Zhang, S. W.; Zhao, J. W.; Ma, P. T.; Chen, H. N.; Niu, J. Y.; Wang, J. P. *Cryst. Growth Des.* **2012**, *12*, 1263−1272.
(43) Zhao, J. W.; Luo, J.; Chen, L. J.; Yuan, J.; Li, H. Y.; Ma, P. T.; Wang, J. P.; Niu, J. Y. *CrystEngComm* **2012**, *14*, 7981−7993.
(44) Zhao, J. W.; Shi, D. Y.; Chen, L. J.; Ma, P. T.; Wang, J. P.; Zhang, J.; Niu, J. Y. *Cryst. Growth Des.* **2013**, *13*, 4368−4377.
(45) Zhao, J. W.; Li, Y. Z.; Ji, F.; Yuan, J.; Chen, L. J.; Yang, G. Y. *Dalton Trans.* **2014**, *43*, 5694−5706.
(46) Fischer, J.; Richard, L.; Weiss, R. *J. Am. Chem. Soc.* **1976**, *98*, 3050−3052.
(47) Bi, L.-H.; Wang, E.-B.; Huang, R.-D. *J. Mol. Struct.* **2000**, *553*, 167−174.
(48) Kortz, U.; Savelieff, M. G.; Bassil, B. S.; Keita, B.; Nadjo, L. *Inorg. Chem.* **2002**, *41*, 783−789.
(49) Volkmer, D.; Bredenkötter, B.; Tellenbröker, J.; Kögerler, P.; Kurth, D. G.; Lehmann, P.; Schnablegger, H.; Schwahn, D.; Piepenbrink, M.; Krebs, B. *J. Am. Chem. Soc.* **2002**, *124*, 10489−10496.
(50) Yamase, T.; Fukaya, K.; Nojiri, H.; Ohshima, Y. *Inorg. Chem.* **2006**, *45*, 7698−7704.
(51) Dolbecq, A.; Compain, J. D.; Mialane, P.; Marrot, J.; Riviere, E.; Sécheresse, F. *Inorg. Chem.* **2008**, *47*, 3371−3378.
(52) McGlone, T.; Vilà-Nadal, L.; Miras, H. N.; Long, D. L.; Poblet, J. M.; Cronin, L. *Dalton Trans.* **2010**, *39*, 11599−11604.
(53) Ibrahim, M.; Mal, S. S.; Bassil, B. S.; Banerjee, A.; Kortz, U. *Inorg. Chem.* **2010**, *50*, 956−960.
(54) Boland, K. S.; Conradson, S. D.; Costello, A. L.; Gaunt, A. J.; Kozimor, S. A.; May, I.; Reilly, S. D.; Schnaars, D. D. *Dalton Trans.* **2012**, *41*, 2003−2010.
(55) Han, Z.-G.; Zhang, Q.-X.; Gao, Y.-Z.; Wu, J. J.; Zhai, X. L. *Dalton Trans.* **2012**, *41*, 1332−1337.
(56) Pilette, M. A.; Floquet, S.; Marrot, J.; Sécheresse, F.; Cadot, E. *Eur. J. Inorg. Chem.* **2013**, 1726−1730.
(57) Carraro, M.; Bassil, B. S.; Sorarù, A.; Berardi, S.; Suchopar, A.; Kortz, U.; Bonchio, M. *Chem. Commun.* **2013**, *49*, 7914−7916.
(58) Bösing, M.; Loose, I.; Pohlmann, H.; Krebs, B. *Chem.—Eur. J.* **1997**, *3*, 1232−1237.
(59) Bösing, M.; Nöh, A.; Loose, I.; Krebs, B. *J. Am. Chem. Soc.* **1998**, *120*, 7252−7259.
(60) Sazani, G.; Dickman, M. H.; Pope, M. T. *Inorg. Chem.* **2000**, *39*, 939−943.
(61) Piepenbrink, M.; Limanski, E. M.; Krebs, B. *Z. Anorg. Allg. Chem.* **2002**, *628*, 1187−1191.
(62) Gaunt, A. J.; May, I.; Copping, R.; Bhatt, A. I.; Collison, D.; Fox, O. D.; Holman, K. T.; Pope, M. T. *Dalton Trans.* **2003**, 3009−3014.
(63) Hussain, F.; Reicke, M.; Kortz, U. *Eur. J. Inorg. Chem.* **2004**, 2733−2738.
(64) Bi, L. H.; Reicke, M.; Kortz, U.; Keita, B.; Nadjo, L.; Clark, R. J. *Inorg. Chem.* **2004**, *43*, 3915−3920.
(65) Ni, L. B.; Patzke, G. R. *CrystEngComm* **2012**, *14*, 6778−6782.
(66) Zhang, D. D.; Wang, C. Z.; Li, S. Z.; Liu, J. P.; Ma, P. T.; Wang, J. P.; Niu, J. Y. *J. Solid State Chem.* **2013**, *98*, 18−23.
(67) Ismail, A. H.; Bassil, B. S.; Römer, I.; Kortz, U. *Z. Anorg. Allg. Chem.* **2013**, *639*, 2510−2515.
(68) Yamase, T. *Chem. Rev.* **1998**, *98*, 307−326.
(69) Benelli, C.; Gatteschi, D. *Chem. Rev.* **2002**, *102*, 2369−2388.
(70) Moll, H. E.; Nohra, B.; Mialane, P.; Marrot, J.; Dupré, N.; Riflade, B.; Malacria, M.; Thorimbert, S.; Hasenknopf, B.; Lacôte, E.; Aparicio, P. A.; López, X.; Poblet, J. M.; Dolbecq, A. *Chem.—Eur. J.* **2011**, *17*, 14129−14138.
(71) Kikukawa, Y.; Yamaguchi, S.; Tsuchida, K.; Nakagawa, Y.; Uehara, K.; Yamaguchi, K.; Mizuno, N. *J. Am. Chem. Soc.* **2008**, *130*, 5472−5478.
(72) *SAINT V 6.01 (NT) Software for the CCD Detector System*; Bruker Analytical X-ray Systems: Madison, WI, 1999.
(73) Sheldrick, G. M. *SADABS: Program for Absorption Correction*; University of Göttingen: Germany, 1997.
(74) Sheldrick, G. M. *SHELXS 97, Program for Crystal Structure Solution*; University of Göttingen: Germany, 1997.
(75) Sheldrick, G. M. *SHELXL 97, Program for Crystal Structure Refinement*; University of Göttingen: Germany, 1997.
(76) Abu-Nawwas, A. A. H.; Cano, J.; Christian, P.; Mallah, T.; Rajaraman, G.; Teat, S. J.; Winpenny, R. E. P.; Yukawa, Y. *Chem. Commun.* **2004**, 314−315.

(77) Torres, J.; Kremer, C.; Kremer, E.; Pardo, H.; Suescun, L.; Mombrffl, A.; DomSnguez, S.; Mederos, A.; Herbst-Irmer, R.; Arrieta, J. M. *J. Chem. Soc., Dalton Trans.* **2002**, 4035−4041.
(78) Zhao, J. W.; Zhang, H. P.; Jia, J.; Zheng, S. T.; Yang, G. Y. *Chem.—Eur. J.* **2007**, *13*, 10030−10045.
(79) Zhao, J. W.; Wang, C. M.; Zhang, J.; Zheng, S. T.; Yang, G. Y. *Chem.—Eur. J.* **2008**, *14*, 9223−9239.
(80) Kortz, U.; Savelieff, M. G.; Ghali, F. Y. A.; Khalil, L. M.; Maalouf, S. A.; Sinno, D. *Angew. Chem., Int. Ed.* **2002**, *41*, 4070−4073.
(81) Duthaler, R. O. *Angew. Chem., Int. Ed.* **2003**, *42*, 975−978.
(82) Hu, S. M.; Du, W. X.; Dai, J. C.; Wu, L. M.; Cui, C. P.; Fu, Z. Y.; Wu, X. T. *J. Chem. Soc., Dalton Trans.* **2001**, 2963−2964.
(83) Ma, B. Q.; Zhang, D. S.; Gao, S.; Jin, T. Z.; Yan, C. H.; Xu, G. X. *Angew. Chem., Int. Ed.* **2000**, *39*, 3644−3646.
(84) Aime, S.; Batsanov, A. S.; Beeby, A.; Botta, M.; Bruce, J. I.; Dickins, R. S.; Howard, J. A. K.; Love, C. S.; Parker, D.; Peacock, R. D.; Puschmann, H. *J. Am. Chem. Soc.* **2002**, *124*, 12697−12705.
(85) Ingleson, M. J.; Barrio, J. P.; Bacsa, J.; Dickinson, C.; Park, H.; Rosseinsky, M. J. *Chem. Commun.* **2008**, 1287−1289.
(86) Li, Z. Y.; Wang, Y. X.; Zhu, J.; Liu, S. Q.; Xin, G.; Zhang, J. J.; Huang, H. Q.; Duan, C. Y. *Cryst. Growth Des.* **2013**, *13*, 3429−3437.
(87) Sadakane, M.; H. Dickman, M.; Pope, M. T. *Inorg. Chem.* **2001**, *40*, 2715−2719.
(88) Müller, A.; Das, S. K.; Kuhlmann, C.; Bögge, H.; Schmidtmann, M.; Diemann, E.; Krickemeyer, E.; Hormes, J.; Modrow, H.; Schindler, M. *Chem. Commun.* **2001**, 655−656.
(89) Kortz, U.; Vaissermann, J.; Thouvenot, R.; Gouzerh, P. *Inorg. Chem.* **2003**, *42*, 1135−1139.
(90) Wang, R. Y.; Jia, D. Z.; Zhang, L.; Liu, L.; Guo, Z. P.; Li, B. Q.; Wang, J. X. *Adv. Funct. Mater.* **2006**, *16*, 687−692.
(91) An, H. Y.; Wang, E. B.; Xiao, D. R.; Li, Y. G.; Su, Z. M.; Xu, L. *Angew. Chem., Int. Ed.* **2006**, *45*, 904−908.
(92) An, H. Y.; Wang, E. B.; Li, Y. G.; Zhang, Z. M.; Xu, L. *Inorg. Chem. Commun.* **2007**, *10*, 299−302.
(93) Liu, D.; Tan, H. Q.; Chen, W. L.; Li, Y. G.; Wang, E. B. *CrystEngComm* **2010**, *12*, 2044−2046.
(94) Zhang, J.; Lan, Q.; Zhang, Z. M.; Liu, Z. J.; Liang, Y.; Wang, E. B. *J. Clust. Sci.* **2014**, *25*, 253−259.
(95) Chen, Z. F.; An, H. Y.; Zhang, H.; Hu, Y. *CrystEngComm* **2013**, *15*, 4711−4720.
(96) Naruke, H.; Iijima, J.; Sanji, T. *Inorg. Chem.* **2011**, *50*, 7535−7539.
(97) Zhao, J. W.; Zhang, J. L.; Li, Y. Z.; Cao, J.; Chen, L. J. *Cryst. Growth Des.* **2014**, *14*, 1467−1475.
(98) Kortz, U. *J. Clust. Sci.* **2003**, *14*, 205−214.
(99) Mialane, P.; Dolbecq, A.; Sécheresse, F. *Chem. Commun.* **2006**, 3477−3485.
(100) Niu, J. Y.; Wang, K.; Chen, H. N.; Zhao, J. W.; Ma, P. T.; Wang, J. P.; Li, M. X.; Bai, Y.; Dang, D. B. *Cryst. Growth Des.* **2009**, *9*, 4362−4372.
(101) Li, C. H.; Huang, K. L.; Chi, Y. N.; Liu, X.; Han, Z. G.; Shen, L.; Hu, C. W. *Inorg. Chem.* **2009**, *48*, 2010−2017.
(102) An, H.; Han, Z.; Xu, T. *Inorg. Chem.* **2010**, *49*, 11403−11414.
(103) Brown, I. D.; Altermatt, D. *Acta Crystallogr.* **1985**, *B41*, 244−247.
(104) Martinez, H.; Benayad, A.; Gonbeau, D.; Vinatier, P.; Pecquenard, B.; Levasseur, A. *Appl. Surf. Sci.* **2004**, *236*, 377−386.
(105) Chen, W. C.; Li, H. L.; Wang, X. L.; Shao, K. Z.; Su, Z. M.; Wang, E. B. *Chem.—Eur. J.* **2013**, *19*, 11007−11015.
(106) Fan, D. W.; Hao, J. C. *J. Phys. Chem. B* **2009**, *113*, 7513−7516.
(107) Tian, P. J.; Cheng, J. S.; Zhang, G. K. *Appl. Surf. Sci.* **2011**, *257*, 4896−4900.
(108) Vercaemst, R.; Poelman, D.; Fiermans, L.; Van Meirhaeghe, R. L.; Laflère, W. H.; Cardon, F. *J. Electron Spectrosc. Relat. Phenom.* **1995**, *74*, 45−56.
(109) Zhang, S. W.; Wang, K.; Zhang, D. D.; Ma, P. T.; Niu, J. Y.; Wang, J. P. *CrystEngComm* **2012**, *14*, 8677−8683.
(110) Tian, S.-B.; Li, Y.-Z.; Zhao, J.-W.; Ma, P.-T.; Chen, L.-J. *Inorg. Chem. Commun.* **2013**, *33*, 99−104.
(111) Loose, I.; Droste, E.; Bösing, M.; Pohlmann, H.; Dickman, M. H.; Rosu, C.; Pope, M. T.; Krebs, B. *Inorg. Chem.* **1999**, *38*, 2688−2694.
(112) Drewes, D.; Limanski, E. M.; Piepenbrink, M.; Krebs, B. *Z. Anorg. Allg. Chem.* **2004**, *630*, 58−62.
(113) Krebs, B.; Droste, E.; Piepenbrink, M.; Vollmer, G. *C. R. Acad. Sci., Ser. IIc: Chim.* **2000**, *3*, 205−210.
(114) Limanski, E. M.; Drewes, D.; Krebs, B. *Z. Anorg. Allg. Chem.* **2004**, *630*, 523−528.
(115) Takacs, A. F.; Schnack, J.; Balasz, I.; Burzo, E.; Kortz, U.; Kuepper, K.; Neumann, M. *J. Appl. Phys.* **2006**, *99*, 08J505.
(116) Chen, L. F.; Zhu, K. K.; Bi, L. H.; Suchopar, A.; Reicke, M.; Mathys, G.; Jaensch, H.; Kortz, U.; Richards, R. M. *Inorg. Chem.* **2007**, *46*, 8457−8459.
(117) Bi, L. H.; Al-Kadamany, G.; Chubarova, E. V.; Dickman, M. H.; Chen, L. F.; Gopala, D. S.; Richards, R. M.; Keita, B.; Nadjo, L.; Jaensch, H.; Mathys, G.; Kortz, U. *Inorg. Chem.* **2009**, *48*, 10068−10077.
(118) Kalinina, I. V.; Izarova, N. V.; Kortz, U. *Inorg. Chem.* **2012**, *51*, 7442−7444.
(119) Zhao, C. C.; Kambara, C. S.; Yang, Y.; Kaledin, A. L.; Musaev, D. G.; Lian, T. Q.; Hill, C. L. *Inorg. Chem.* **2013**, *52*, 671−678.
(120) Moulton, B.; Zaworotko, M. J. *Chem. Rev.* **2001**, *101*, 1629−1658.
(121) Yaghi, O. M.; O'Keeffe, M.; Ockwig, N. W.; Chae, H. K.; Eddaoudi, M.; Kim, J. *Nature* **2003**, *423*, 705−714.
(122) Coronado, E.; Gómez-García, C. J. *Chem. Rev.* **1998**, *98*, 273−296.
(123) Mizuno, N.; Misono, M. *Chem. Rev.* **1998**, *98*, 199−218.
(124) Zheng, P. Q.; Ren, Y. P.; Long, L. S.; Huang, R. B.; Zheng, L. S. *Inorg. Chem.* **2005**, *44*, 1190−1192.
(125) Armelao, L.; Quici, S.; Barigelletti, F.; Accorsi, G.; Bottaro, G.; Cavazzini, M.; Tondello, E. *Coord. Chem. Rev.* **2010**, *254*, 487−505.
(126) Sopasis, G. J.; Orfanoudaki, M.; Zarmpas, P.; Philippidis, A.; Siczek, M.; Lis, T.; O'Brien, J. R.; Milios, C. J. *Inorg. Chem.* **2012**, *51*, 1170−1179.
(127) Cai, S.-L.; Zheng, S.-R.; Wen, Z.-Z.; Fan, J.; Zhang, W.-G. *Cryst. Growth Des.* **2012**, *12*, 5737−5745.
(128) Ricci, R. W.; Kilichowski, K. B. *J. Phys. Chem.* **1974**, *78*, 1953−1956.
(129) Xu, Q.; Li, L.; Liu, X.; Xu, R. *Chem. Mater.* **2002**, *14*, 549−555.
(130) Kirby, A. F.; Richardson, F. S. *J. Phys. Chem.* **1983**, *87*, 2544−2556.
(131) Stouwdam, J. W.; van Veggel, F. C. J. M. *Nano Lett.* **2002**, *2*, 733−737.
(132) Zhang, T.; Spitz, C.; Antonietti, M.; Faul, C. F. J. *Chem.—Eur. J.* **2005**, *11*, 1001−1009.
(133) Mialane, P.; Lisnard, L.; Mallard, A.; Marrot, J.; Antic-Fidancev, E.; Aschehoug, P.; Vivien, D.; Sécheresse, F. *Inorg. Chem.* **2003**, *42*, 2102−2108.
(134) Toth, J. E.; Anson, F. C. *J. Am. Chem. Soc.* **1989**, *111*, 2444−2451.
(135) Rüther, T.; Hultgren, V. M.; Timko, B. P.; Bond, A. M.; Jackson, W. R.; Wedd, A. G. *J. Am. Chem. Soc.* **2003**, *125*, 10133−10143.
(136) Keita, B.; de Oliveira, P.; Nadjo, L.; Kortz, U. *Chem.—Eur. J.* **2007**, *13*, 5480−5491.
(137) Zhang, Z.-M.; Qi, Y.-F.; Qin, C.; Li, Y. G.; Wang, E. B.; Wang, X. L.; Su, Z. M.; Xu, L. *Inorg. Chem.* **2007**, *46*, 8162−8169.
(138) Wang, X. L.; Wang, E. B.; Lan, Y.; Hu, C. W. *Electroanalysis* **2002**, *14*, 1116−1121.
(139) Wang, X. L.; Han, Z. B.; Wang, E. B.; Zhang, H.; Hu, C. W. *Electroanalysis* **2003**, *15*, 1460−1464.
(140) Nohra, B.; El Moll, H.; Rodriguez Albelo, L. M.; Mialane, P.; Marrot, J.; Mellot-Draznieks, C.; O'Keeffe, M.; Biboum, R. N.; Lemaire, J.; Keita, B.; Nadjo, L.; Dolbecq, A. *J. Am. Chem. Soc.* **2011**, *133*, 13363−13374.
(141) Sadakane, M.; Stechhan, E. *Chem. Rev.* **1998**, *98*, 219−238.

(142) Toth, J. E.; Anson, F. C. *J. Electroanal. Chem.* **1988**, *256*, 361−370.
(143) Sadakane, M.; Steckhan, E. *Chem. Rev.* **1998**, *98*, 219−237.
(144) Anwar, N.; Vagin, M.; Laffir, F.; Armstrong, G.; Dickinson, C.; McCormac, T. *Analyst* **2012**, *137*, 624−630.
(145) Han, Z.; Zhao, Y.; Peng, J.; Liu, Q.; Wang, E. *Electrochim. Acta* **2005**, *51*, 218−224.
(146) Bi, L. H.; Kortz, U.; Nellutla, S.; Stowe, A. C.; Tol, J. V.; Dalal, N. S.; Keita, B.; Nadjo, L. *Inorg. Chem.* **2005**, *44*, 896−903.
(147) Mbomekalle, I. M.; Mialane, P.; Dolbecq, A.; Marrot, J.; Sécheresse, F.; Berthet, P.; Keita, B.; Nadjo, L. *Eur. J. Inorg. Chem.* **2009**, 5194−5204.
(148) Ammam, M.; Mbomekalle, I. M.; Keita, B.; Nadjo, L.; Anderson, T. M.; Zhang, X.; Hardcastlec, K. I.; Hill, C. L.; Fransaer, J. *J. Electroanal. Chem.* **2010**, *647*, 97−102.
(149) Moore, M. M.; Chen, T. *Toxicology* **2006**, *221*, 190−196.
(150) Bonacquisti, T. P. *Toxicology* **2006**, *221*, 145−148.
(151) Rodriguez-Albelo, L. M.; Ruiz-Salvador, A. R.; Sampieri, A.; Lewis, D. W.; Gómez, A.; Nohra, B.; Mialane, P.; Marrot, J.; Sécheresse, F.; Mellot-Draznieks, C.; Biboum, R. N.; Keita, B.; Nadjo, L.; Dolbecq, A. *J. Am. Chem. Soc.* **2009**, *131*, 16078−16087.
(152) Wang, J.; Lin, Y.; Chen, L. *Analyst* **1993**, *118*, 277−280.
(153) Bi, L. H.; Foster, K.; McCormac, T.; Dempsey, E. *J. Electroanal. Chem.* **2007**, *65*, 24−30.
(154) Wang, S.; Pang, Z.; Smith, K. D. L.; Wagner, M. J. *J. Chem. Soc., Dalton Trans.* **1994**, 955−964.
(155) Kahn, O. *Adv. Inorg. Chem.* **1995**, *43*, 179−259.
(156) Rizzi, A. C.; Calvo, R.; Baggio, R.; Garland, M. T.; Peña, O.; Perec, M. *Inorg. Chem.* **2002**, *41*, 5609−5614.
(157) Kahn, M. L.; Sutter, J.; Golhen, S.; Guionneau, P.; Ouahab, L.; Kahn, O.; Chasseau, D. *J. Am. Chem. Soc.* **2000**, *122*, 3413−3421.
(158) Sun, Y. Q.; Zhang, J.; Chen, Y. M.; Yang, G. Y. *Angew. Chem., Int. Ed.* **2005**, *44*, 5810−5814.
(159) Figuerola, A.; Ribas, J.; Llunell, M.; Casanova, D.; Maestro, M.; Alvarez, S.; Diaz, C. *Inorg. Chem.* **2005**, *44*, 6939−6948.
(160) Li, Y.; Zheng, F. K.; Liu, X.; Zou, W. Q.; Guo, G. C.; Lu, C. Z.; Huang, J. S. *Inorg. Chem.* **2006**, *45*, 6308−6316.
(161) Arumuganathan, T.; Das, S. K. *Inorg. Chem.* **2009**, *48*, 496−507.
(162) Xu, J. X.; Ma, Y.; Liao, D. Z.; Xu, G. F.; Tang, J. K.; Wang, C.; Zhou, N.; Yan, S. P.; Cheng, P.; Li, L. C. *Inorg. Chem.* **2009**, *48*, 8890−8896.
(163) Ishikawa, N.; Sugita, M.; Okubo, T.; Tanaka, N.; Lino, T.; Kaizu, Y. *Inorg. Chem.* **2003**, *42*, 2440−2446.
(164) Ritchie, C.; Speldrich, M.; Gable, R. W.; Sorace, L.; Kögerler, P.; Boskovic, C. *Inorg. Chem.* **2011**, *50*, 7004−7014.
(165) Guillou, O.; Bergerat, P.; Kahn, O.; Bakalbassis, E.; Boubekeur, K.; Batail, P.; Guillot, M. *Inorg. Chem.* **1992**, *31*, 110−114.
(166) Mondal, K. C.; Kostakis, G. E.; Lan, Y.; Wernsdorfer, W.; Anson, C. E.; Powell, A. K. *Inorg. Chem.* **2011**, *50*, 11604−11611.
(167) Rinck, J.; Novitchi, G.; Heuvel, W. V. D.; Ungur, L.; Lan, Y.; Wernsdorfer, W.; Anson, C. E.; Chibotaru, L. F.; Powell, A. K. *Angew. Chem., Int. Ed.* **2010**, *49*, 7583−7587.
(168) Sun, Y. G.; Li, J.; Li, K. L.; Xu, Z. H.; Ding, F.; Ren, B. Y.; Wang, S. J.; You, L. X.; Xiong, G.; Smet, P. F. *CrystEngComm* **2014**, *16*, 1777−1785.